SLAC-PUB-8530
BABAR-CONF-00/00
hep-ex/0008052
August, 2000

A measurement of the $B^0\overline{B}^0$ oscillation frequency and determination of flavor-tagging efficiency using semileptonic and hadronic B^0 decays

The *BABAR* Collaboration

Abstract

$B^0\overline{B}^0$ flavor oscillations are studied in e^+e^- annihilation data collected with the *BABAR* detector at center-of-mass energies near the $\Upsilon(4S)$ resonance. One B is reconstructed in a hadronic or semileptonic decay mode, and the flavor of the other B in the event is determined with a tagging algorithm that exploits the relation between the flavor of the heavy quark and the charges of its decay products. Tagging performance is characterized by an efficiency ϵ_i and a probability for mis-identification, w_i, for each tagging category. We report a determination of the wrong-tag probabilities, w_i, and a preliminary result for the time-dependent $B^0\overline{B}^0$ oscillation frequency, $\Delta m_d = 0.512 \pm 0.017 \pm 0.022\ \hbar\,\mathrm{ps}^{-1}$.

Submitted to the 30^{th} International Conference on High Energy Physics,
7/27/2000—8/2/2000, Osaka, Japan

Stanford Linear Accelerator Center, Stanford University, Stanford, CA 94309

Work supported in part by Department of Energy contract DE-AC03-76SF00515.

The *BABAR* Collaboration

B. Aubert, A. Boucham, D. Boutigny, I. De Bonis, J. Favier, J.-M. Gaillard, F. Galeazzi, A. Jeremie, Y. Karyotakis, J. P. Lees, P. Robbe, V. Tisserand, K. Zachariadou

Lab de Phys. des Particules, F-74941 Annecy-le-Vieux, CEDEX, France

A. Palano

Università di Bari, Dipartimento di Fisica and INFN, I-70126 Bari, Italy

G. P. Chen, J. C. Chen, N. D. Qi, G. Rong, P. Wang, Y. S. Zhu

Institute of High Energy Physics, Beijing 100039, China

G. Eigen, P. L. Reinertsen, B. Stugu

University of Bergen, Inst. of Physics, N-5007 Bergen, Norway

B. Abbott, G. S. Abrams, A. W. Borgland, A. B. Breon, D. N. Brown, J. Button-Shafer, R. N. Cahn, A. R. Clark, Q. Fan, M. S. Gill, S. J. Gowdy, Y. Groysman, R. G. Jacobsen, R. W. Kadel, J. Kadyk, L. T. Kerth, S. Kluth, J. F. Kral, C. Leclerc, M. E. Levi, T. Liu, G. Lynch, A. B. Meyer, M. Momayezi, P. J. Oddone, A. Perazzo, M. Pripstein, N. A. Roe, A. Romosan, M. T. Ronan, V. G. Shelkov, P. Strother, A. V. Telnov, W. A. Wenzel

Lawrence Berkeley National Lab, Berkeley, CA 94720, USA

P. G. Bright-Thomas, T. J. Champion, C. M. Hawkes, A. Kirk, S. W. O'Neale, A. T. Watson, N. K. Watson

University of Birmingham, Birmingham, B15 2TT, UK

T. Deppermann, H. Koch, J. Krug, M. Kunze, B. Lewandowski, K. Peters, H. Schmuecker, M. Steinke

Ruhr Universität Bochum, Inst. f. Experimentalphysik 1, D-44780 Bochum, Germany

J. C. Andress, N. Chevalier, P. J. Clark, N. Cottingham, N. De Groot, N. Dyce, B. Foster, A. Mass, J. D. McFall, D. Wallom, F. F. Wilson

University of Bristol, Bristol BS8 lTL, UK

K. Abe, C. Hearty, T. S. Mattison, J. A. McKenna, D. Thiessen

University of British Columbia, Vancouver, BC, Canada V6T 1Z1

B. Camanzi, A. K. McKemey, J. Tinslay

Brunel University, Uxbridge, Middlesex UB8 3PH, UK

V. E. Blinov, A. D. Bukin, D. A. Bukin, A. R. Buzykaev, M. S. Dubrovin, V. B. Golubev, V. N. Ivanchenko, A. A. Korol, E. A. Kravchenko, A. P. Onuchin, A. A. Salnikov, S. I. Serednyakov, Yu. I. Skovpen, A. N. Yushkov

Budker Institute of Nuclear Physics, Siberian Branch of Russian Academy of Science, Novosibirsk 630090, Russia

A. J. Lankford, M. Mandelkern, D. P. Stoker

University of California at Irvine, Irvine, CA 92697, USA

A. Ahsan, K. Arisaka, C. Buchanan, S. Chun

University of California at Los Angeles, Los Angeles, CA 90024, USA

J. G. Branson, R. Faccini,[1] D. B. MacFarlane, Sh. Rahatlou, G. Raven, V. Sharma

University of California at San Diego, La Jolla, CA 92093, USA

C. Campagnari, B. Dahmes, P. A. Hart, N. Kuznetsova, S. L. Levy, O. Long, A. Lu, J. D. Richman, W. Verkerke, M. Witherell, S. Yellin

University of California at Santa Barbara, Santa Barbara, CA 93106, USA

J. Beringer, D. E. Dorfan, A. Eisner, A. Frey, A. A. Grillo, M. Grothe, C. A. Heusch, R. P. Johnson, W. Kroeger, W. S. Lockman, T. Pulliam, H. Sadrozinski, T. Schalk, R. E. Schmitz, B. A. Schumm, A. Seiden, M. Turri, D. C. Williams

University of California at Santa Cruz, Institute for Particle Physics, Santa Cruz, CA 95064, USA

E. Chen, G. P. Dubois-Felsmann, A. Dvoretskii, D. G. Hitlin, Yu. G. Kolomensky, S. Metzler, J. Oyang, F. C. Porter, A. Ryd, A. Samuel, M. Weaver, S. Yang, R. Y. Zhu

California Institute of Technology, Pasadena, CA 91125, USA

R. Aleksan, G. De Domenico, A. de Lesquen, S. Emery, A. Gaidot, S. F. Ganzhur, G. Hamel de Monchenault, W. Kozanecki, M. Langer, G. W. London, B. Mayer, B. Serfass, G. Vasseur, C. Yeche, M. Zito

Centre d'Etudes Nucléaires, Saclay, F-91191 Gif-sur-Yvette, France

S. Devmal, T. L. Geld, S. Jayatilleke, S. M. Jayatilleke, G. Mancinelli, B. T. Meadows, M. D. Sokoloff

University of Cincinnati, Cincinnati, OH 45221, USA

J. Blouw, J. L. Harton, M. Krishnamurthy, A. Soffer, W. H. Toki, R. J. Wilson, J. Zhang

Colorado State University, Fort Collins, CO 80523, USA

S. Fahey, W. T. Ford, F. Gaede, D. R. Johnson, A. K. Michael, U. Nauenberg, A. Olivas, H. Park, P. Rankin, J. Roy, S. Sen, J. G. Smith, D. L. Wagner

University of Colorado, Boulder, CO 80309, USA

T. Brandt, J. Brose, G. Dahlinger, M. Dickopp, R. S. Dubitzky, M. L. Kocian, R. Müller-Pfefferkorn, K. R. Schubert, R. Schwierz, B. Spaan, L. Wilden

Technische Universität Dresden, Inst. f. Kern- u. Teilchenphysik, D-01062 Dresden, Germany

L. Behr, D. Bernard, G. R. Bonneaud, F. Brochard, J. Cohen-Tanugi, S. Ferrag, E. Roussot, C. Thiebaux, G. Vasileiadis, M. Verderi

Ecole Polytechnique, Lab de Physique Nucléaire H. E., F-91128 Palaiseau, France

A. Anjomshoaa, R. Bernet, F. Di Lodovico, F. Muheim, S. Playfer, J. E. Swain

University of Edinburgh, Edinburgh EH9 3JZ, UK

C. Bozzi, S. Dittongo, M. Folegani, L. Piemontese

Università di Ferrara, Dipartimento di Fisica and INFN, I-44100 Ferrara, Italy

E. Treadwell

Florida A&M University, Tallahassee, FL 32307, USA

[1]Jointly appointed with Università di Roma La Sapienza, Dipartimento di Fisica and INFN, I-00185 Roma, Italy

R. Baldini-Ferroli, A. Calcaterra, R. de Sangro, D. Falciai, G. Finocchiaro, P. Patteri, I. M. Peruzzi,[2] M. Piccolo, A. Zallo

Laboratori Nazionali di Frascati dell'INFN, I-00044 Frascati, Italy

S. Bagnasco, A. Buzzo, R. Contri, G. Crosetti, P. Fabbricatore, S. Farinon, M. Lo Vetere, M. Macri, M. R. Monge, R. Musenich, R. Parodi, S. Passaggio, F. C. Pastore, C. Patrignani, M. G. Pia, C. Priano, E. Robutti, A. Santroni

Università di Genova, Dipartimento di Fisica and INFN, I-16146 Genova, Italy

J. Cochran, H. B. Crawley, P.-A. Fischer, J. Lamsa, W. T. Meyer, E. I. Rosenberg

Iowa State University, Ames, IA 50011-3160, USA

R. Bartoldus, T. Dignan, R. Hamilton, U. Mallik

University of Iowa, Iowa City, IA 52242, USA

C. Angelini, G. Batignani, S. Bettarini, M. Bondioli, M. Carpinelli, F. Forti, M. A. Giorgi, A. Lusiani, M. Morganti, E. Paoloni, M. Rama, G. Rizzo, F. Sandrelli, G. Simi, G. Triggiani

Università di Pisa, Scuola Normale Superiore, and INFN, I-56010 Pisa, Italy

M. Benkebil, G. Grosdidier, C. Hast, A. Hoecker, V. LePeltier, A. M. Lutz, S. Plaszczynski, M. H. Schune, S. Trincaz-Duvoid, A. Valassi, G. Wormser

LAL, F-91898 ORSAY Cedex, France

R. M. Bionta, V. Brigljević, O. Fackler, D. Fujino, D. J. Lange, M. Mugge, X. Shi, T. J. Wenaus, D. M. Wright, C. R. Wuest

Lawrence Livermore National Laboratory, Livermore, CA 94550, USA

M. Carroll, J. R. Fry, E. Gabathuler, R. Gamet, M. George, M. Kay, S. McMahon, T. R. McMahon, D. J. Payne, C. Touramanis

University of Liverpool, Liverpool L69 3BX, UK

M. L. Aspinwall, P. D. Dauncey, I. Eschrich, N. J. W. Gunawardane, R. Martin, J. A. Nash, P. Sanders, D. Smith

University of London, Imperial College, London, SW7 2BW, UK

D. E. Azzopardi, J. J. Back, P. Dixon, P. F. Harrison, P. B. Vidal, M. I. Williams

University of London, Queen Mary and Westfield College, London, E1 4NS, UK

G. Cowan, M. G. Green, A. Kurup, P. McGrath, I. Scott

University of London, Royal Holloway and Bedford New College, Egham, Surrey TW20 0EX, UK

D. Brown, C. L. Davis, Y. Li, J. Pavlovich, A. Trunov

University of Louisville, Louisville, KY 40292, USA

J. Allison, R. J. Barlow, J. T. Boyd, J. Fullwood, A. Khan, G. D. Lafferty, N. Savvas, E. T. Simopoulos, R. J. Thompson, J. H. Weatherall

University of Manchester, Manchester M13 9PL, UK

[2]Jointly appointed with Univ. di Perugia, I-06100 Perugia, Italy

C. Dallapiccola, A. Farbin, A. Jawahery, V. Lillard, J. Olsen, D. A. Roberts
University of Maryland, College Park, MD 20742, USA

B. Brau, R. Cowan, F. Taylor, R. K. Yamamoto
Massachusetts Institute of Technology, Lab for Nuclear Science, Cambridge, MA 02139, USA

G. Blaylock, K. T. Flood, S. S. Hertzbach, R. Kofler, C. S. Lin, S. Willocq, J. Wittlin
University of Massachusetts, Amherst, MA 01003, USA

P. Bloom, D. I. Britton, M. Milek, P. M. Patel, J. Trischuk
McGill University, Montreal, PQ, Canada H3A 2T8

F. Lanni, F. Palombo
Università di Milano, Dipartimento di Fisica and INFN, I-20133 Milano, Italy

J. M. Bauer, M. Booke, L. Cremaldi, R. Kroeger, J. Reidy, D. Sanders, D. J. Summers
University of Mississippi, University, MS 38677, USA

J. F. Arguin, J. P. Martin, J. Y. Nief, R. Seitz, P. Taras, A. Woch, V. Zacek
Université de Montreal, Lab. Rene J. A. Levesque, Montreal, QC, Canada, H3C 3J7

H. Nicholson, C. S. Sutton
Mount Holyoke College, South Hadley, MA 01075, USA

N. Cavallo, G. De Nardo, F. Fabozzi, C. Gatto, L. Lista, D. Piccolo, C. Sciacca
Università di Napoli Federico II, Dipartimento di Scienze Fisiche and INFN, I-80126 Napoli, Italy

M. Falbo
Northern Kentucky University, Highland Heights, KY 41076, USA

J. M. LoSecco
University of Notre Dame, Notre Dame, IN 46556, USA

J. R. G. Alsmiller, T. A. Gabriel, T. Handler
Oak Ridge National Laboratory, Oak Ridge, TN 37831, USA

F. Colecchia, F. Dal Corso, G. Michelon, M. Morandin, M. Posocco, R. Stroili, E. Torassa, C. Voci
Università di Padova, Dipartimento di Fisica and INFN, I-35131 Padova, Italy

M. Benayoun, H. Briand, J. Chauveau, P. David, C. De la Vaissière, L. Del Buono, O. Hamon, F. Le Diberder, Ph. Leruste, J. Lory, F. Martinez-Vidal, L. Roos, J. Stark, S. Versillé
Universités Paris VI et VII, Lab de Physique Nucléaire H. E., F-75252 Paris, Cedex 05, France

P. F. Manfredi, V. Re, V. Speziali
Università di Pavia, Dipartimento di Elettronica and INFN, I-27100 Pavia, Italy

E. D. Frank, L. Gladney, Q. H. Guo, J. H. Panetta
University of Pennsylvania, Philadelphia, PA 19104, USA

M. Haire, D. Judd, K. Paick, L. Turnbull, D. E. Wagoner
Prairie View A&M University, Prairie View, TX 77446, USA

J. Albert, C. Bula, M. H. Kelsey, C. Lu, K. T. McDonald, V. Miftakov, S. F. Schaffner, A. J. S. Smith, A. Tumanov, E. W. Varnes

Princeton University, Princeton, NJ 08544, USA

G. Cavoto, F. Ferrarotto, F. Ferroni, K. Fratini, E. Lamanna, E. Leonardi, M. A. Mazzoni, S. Morganti, G. Piredda, F. Safai Tehrani, M. Serra

Università di Roma La Sapienza, Dipartimento di Fisica and INFN, I-00185 Roma, Italy

R. Waldi

Universität Rostock, D-18051 Rostock, Germany

P. F. Jacques, M. Kalelkar, R. J. Plano

Rutgers University, New Brunswick, NJ 08903, USA

T. Adye, U. Egede, B. Franek, N. I. Geddes, G. P. Gopal

Rutherford Appleton Laboratory, Chilton, Didcot, Oxon., OX11 0QX, UK

N. Copty, M. V. Purohit, F. X. Yumiceva

University of South Carolina, Columbia, SC 29208, USA

I. Adam, P. L. Anthony, F. Anulli, D. Aston, K. Baird, E. Bloom, A. M. Boyarski, F. Bulos, G. Calderini, M. R. Convery, D. P. Coupal, D. H. Coward, J. Dorfan, M. Doser, W. Dunwoodie, T. Glanzman, G. L. Godfrey, P. Grosso, J. L. Hewett, T. Himel, M. E. Huffer, W. R. Innes, C. P. Jessop, P. Kim, U. Langenegger, D. W. G. S. Leith, S. Luitz, V. Luth, H. L. Lynch, G. Manzin, H. Marsiske, S. Menke, R. Messner, K. C. Moffeit, M. Morii, R. Mount, D. R. Muller, C. P. O'Grady, P. Paolucci, S. Petrak, H. Quinn, B. N. Ratcliff, S. H. Robertson, L. S. Rochester, A. Roodman, T. Schietinger, R. H. Schindler, J. Schwiening, G. Sciolla, V. V. Serbo, A. Snyder, A. Soha, S. M. Spanier, A. Stahl, D. Su, M. K. Sullivan, M. Talby, H. A. Tanaka, J. Va'vra, S. R. Wagner, A. J. R. Weinstein, W. J. Wisniewski, C. C. Young

Stanford Linear Accelerator Center, Stanford, CA 94309, USA

P. R. Burchat, C. H. Cheng, D. Kirkby, T. I. Meyer, C. Roat

Stanford University, Stanford, CA 94305-4060, USA

A. De Silva, R. Henderson

TRIUMF, Vancouver, BC, Canada V6T 2A3

W. Bugg, H. Cohn, E. Hart, A. W. Weidemann

University of Tennessee, Knoxville, TN 37996, USA

T. Benninger, J. M. Izen, I. Kitayama, X. C. Lou, M. Turcotte

University of Texas at Dallas, Richardson, TX 75083, USA

F. Bianchi, M. Bona, B. Di Girolamo, D. Gamba, A. Smol, D. Zanin

Università di Torino, Dipartimento di Fisica Sperimentale and INFN, I-10125 Torino, Italy

L. Bosisio, G. Della Ricca, L. Lanceri, A. Pompili, P. Poropat, M. Prest, E. Vallazza, G. Vuagnin

Università di Trieste, Dipartimento di Fisica and INFN, I-34127 Trieste, Italy

R. S. Panvini

Vanderbilt University, Nashville, TN 37235, USA

C. M. Brown, P. D. Jackson, R. Kowalewski, J. M. Roney
University of Victoria, Victoria, BC, Canada V8W 3P6

H. R. Band, E. Charles, S. Dasu, P. Elmer, J. R. Johnson, J. Nielsen, W. Orejudos, Y. Pan, R. Prepost, I. J. Scott, J. Walsh, S. L. Wu, Z. Yu, H. Zobernig
University of Wisconsin, Madison, WI 53706, USA

1 Introduction

The phenomenon of particle–anti-particle mixing in the neutral B meson system was first observed almost fifteen years ago [1], [2]. The oscillation frequency in $B^0\overline{B}^0$ mixing[1] has been extensively studied with both time-integrated and time-dependent techniques [3]. In this paper we present a preliminary measurement of time-dependent mixing performed at the PEP-II asymmetric e^+e^- collider, where resonant production of the $\Upsilon(4S)$ provides a copious source of $B^0\overline{B}^0$ pairs moving along the beam axis (z direction) with a Lorentz boost of $\beta\gamma = 0.56$. The typical separation between the two B decay vertices is $\Delta z = \beta\gamma c\tau_B = 260\,\mu$m, where $\tau_B = 1.548 \pm 0.032$ ps is the B^0 lifetime [3]. The $B^0\overline{B}^0$ mixing probability is a function of Δm_d, the difference between the mass eigenstates B^0_H and B^0_L, and the time between the B decays, $\Delta t = \Delta z/\beta\gamma c$:

$$Prob(B^0 \to \overline{B}^0) \propto \mathrm{e}^{-|\Delta t|/\tau_B}(1 - \cos\Delta m_d \Delta t). \tag{1}$$

In the Standard Model, $B^0\overline{B}^0$ mixing occurs through second-order weak diagrams involving the exchange of up-type quarks, with the top quark contributing the dominant amplitude. A measurement of Δm_d is therefore sensitive to the value of the Cabbibo-Kobayashi-Maskawa matrix [4] element V_{td}. At present the sensitivity to V_{td} is not limited by experimental precision on Δm_d, but by other uncertainties in the calculation, in particular the quantity $f_B^2 B_B$, where f_B is the B^0 decay constant, and B_B is the so-called bag factor, representing the strong interaction matrix elements.

In this analysis, we study the time-dependent probability to observe $B^0\overline{B}^0$, B^0B^0 and $\overline{B}^0\overline{B}^0$ pairs produced in $\Upsilon(4S)$ decay. We reconstruct one B in a flavor eigenstate, and use the remaining particles from the decay of the other B to identify, or "tag", its flavor. The charges of identified leptons and kaons are the primary indicators of the flavor of the tagging B, but other particles also carry flavor information that can be identified with a neural network algorithm. The tagging algorithm used in this analysis is identical to that employed by *BABAR* in *CP* violation studies, in which one B is fully reconstructed in a *CP* eigenstate [5].

Considering the $B^0\overline{B}^0$ system as a whole, one can classify the tagged events as *mixed* or *unmixed* depending on whether the reconstructed B, referred to as B_{rec}, has the same or the opposite flavor as the tagging B, referred to as B_{tag}. If the flavor tagging were perfect, the asymmetry

$$a(\Delta t) = \frac{N_{\rm unmix} - N_{\rm mix}}{N_{\rm unmix} + N_{\rm mix}} \tag{2}$$

plotted as a function of Δt would describe a cosine function with unit amplitude. However, the tagging algorithm incorrectly identifies the tag with a probability w. This mistag rate reduces the amplitude of the oscillation by a "dilution factor" $\mathcal{D} = (1 - 2w)$. When more than one type of flavor tag is employed, each will have its own mistag rate, w_i. A simultaneous fit to the mixing frequency and its amplitude allows the determination of both Δm_d and the mistag rates, w_i.

Neglecting any background contributions, the probability density functions (PDF's) for the mixed ($-$) and unmixed ($+$) events can be expressed as the convolution of the oscillatory component $h_\pm$, with a time resolution function $\mathcal{R}(\Delta t|\hat{a})$:

$$\mathcal{H}_\pm(\,\Delta t; \Gamma,\, \Delta m_d,\, \mathcal{D},\, \hat{a}\,) = h_\pm(\,\Delta t; \Gamma,\, \Delta m_d,\, \mathcal{D}) \otimes \mathcal{R}(\Delta t; \hat{a}), \tag{3}$$

[1] The symbol B^0 refers to the B_d meson; charge conjugate modes are implied throughout this paper.

where $\hat{a}$ are the parameters of the resolution function and

$$h_{\pm}(\,\Delta t;\Gamma,\,\Delta m_d,\,\mathcal{D}\,) = \frac{1}{4}\,\Gamma\,\mathrm{e}^{-\Gamma|\Delta t|}\,\left[\,1\,\pm\,\mathcal{D}\cos\Delta m_d\,\Delta t\,\right]. \tag{4}$$

The log-likelihood function is then constructed from the sum of $\mathcal{H}_{\pm}$ over all mixed and unmixed events, and over the different tag types, i, each with its own characteristic dilution factor $\mathcal{D}_i$:

$$\ln\mathcal{L} = \sum_{i}^{\text{tagging}}\left[\sum_{\text{unmixed}}\ln\mathcal{H}_{+}(\,\Delta t;\Gamma,\,\Delta m_d,\,\mathcal{D}_i,\,\hat{a}_i\,) + \sum_{\text{mixed}}\ln\mathcal{H}_{-}(\,\Delta t;\Gamma,\,\Delta m_d,\,\mathcal{D}_i,\,\hat{a}_i\,)\right]. \tag{5}$$

The log-likelihood is maximized to extract the dilutions $\mathcal{D}_i$ and, simultaneously, the mixing parameter Δm_d. The correlation between these parameters is small, because the rate of mixed events at low values of Δt, where the $B^0\overline{B}^0$ mixing probability is small, is principally governed by the mistag rate. Conversely, the sensitivity to Δm_d increases at larger values of Δt; when Δt is approximately twice the B lifetime, half of the neutral Bs will have oscillated.

Alternatively, the mistag rate can be extracted in a time-independent analysis. Neglecting possible background contributions and assuming the B_{rec} flavor is correctly identified, one can express the observed time-integrated fraction of mixed events χ_{obs} as a function of the $B^0\overline{B}^0$ mixing probability χ_d :

$$\chi_{obs} = \chi_d + (1-2\chi_d)\,w, \tag{6}$$

where $\chi_d = \frac{1}{2}\,x_d^2/(1+x_d^2)$ and $x_d = \Delta m_d/\Gamma$. The current world average for χ_d is 0.174 ± 0.009 [3]. Because decay time information is available in *BABAR*, we can improve the statistical precision on w by selecting only events that fall into an optimized time interval, $|\Delta t| < t'$, where t' is the value of $|\Delta t|$ above which the integrated number of mixed events equals the integrated number of unmixed events. Through the use of an optimized Δt interval this method achieves nearly the same statistical precision on w that is obtained in a full time-dependent likelihood fit.

2 The *BABAR* detector and data set

The data used in this analysis were collected with the *BABAR* detector [6] at the PEP-II storage ring in the period January–June, 2000. The total integrated luminosity of the data set is $8.9\,\text{fb}^{-1}$ collected near the $\Upsilon(4S)$ resonance and $0.8\,\text{fb}^{-1}$ collected 40 MeV below the $\Upsilon(4S)$ resonance (off-resonance data). The corresponding number of produced $B\overline{B}$ pairs is estimated to be about $(10.1\pm 0.4)\times 10^6$.

The *BABAR* detector is described in more detail elsewhere [6]. For this analysis, the most important detector capabilities include charged-particle tracking, vertexing and particle identification. Charged particles are detected and their momenta measured by a combination of a central drift chamber (DCH) filled with a helium-based gas and a five-layer, double-sided silicon vertex tracker (SVT), immersed in a 1.5 T axial field produced by a superconducting magnet. The charged-particle momentum resolution is given by $(\delta p_T/p_T)^2 = (0.0015\,p_T)^2 + (0.005)^2$, where p_T is in GeV/c. The SVT, with typical $10\,\mu$m single-hit resolution, provides vertex information in both the transverse plane and in z. The B meson decay vertex resolution is typically $50\,\mu$m in z for a fully reconstructed B meson and about 100 to $150\,\mu$m for the companion (unreconstructed) B meson in the event. Beyond the outer radius of the DCH is a detector of internally reflected Cherenkov radiation (DIRC) which is used primarily for charged hadron identification. The device consists of quartz bars in which Cherenkov light is produced as relativistic charged particles traverse the

material. The light is internally reflected, and the Cherenkov rings are measured with an array of photomultiplier tubes mounted on the rear of the detector. A CsI(Tl) crystal electromagnetic calorimeter (EMC) is used to detect photons, and neutral hadrons, and also for electron identification. The EMC is surrounded by a superconducting coil which provides a 1.5 T magnetic field. The Instrumented Flux Return (IFR) consists of multiple layers of resistive plate chambers interleaved with the flux return iron and is used in the identification of muons and neutral hadrons.

3 Particle identification

Identification of electrons, muons and kaons is an essential ingredient of both B reconstruction and flavor tagging. As noted above, the *BABAR* detector has several systems that contribute to particle identification, including the measured $\mathrm{d}E/\mathrm{d}x$ in the SVT and the drift chamber, Cherenkov angle determination in the DIRC, electromagnetic energy measurement in the CsI calorimeter and detection of penetrating particles in the IFR. In this section we describe in detail the selections that are employed to identify particles by species, both for the purposes of flavor tagging and for B reconstruction, where the latter typically employs looser selection criteria. We also include the preliminary average values for efficiency and pion misidentification probabilities, as determined from data.

3.1 Electron identification

For tagging purposes, an electron candidate must be matched to an electromagnetic cluster in the CsI calorimeter consisting of at least three crystals, and the ratio of the cluster energy to the track momentum E/p must be between 0.88 and 1.3. Cuts [6] based on electromagnetic shower shape are also used in identifying electron candidates. In addition the electron candidate track is required to have a specific ionization ($\mathrm{d}E/\mathrm{d}x$) measurement in the drift chamber consistent with that of an electron, and, if measured, the Cherenkov angle in the DIRC is required to be consistent with that of an ultra-relativistic particle. The electron efficiency and pion misidentification probabilities for this selection are about 92% and 0.3%, respectively.

A somewhat looser electron selection is used in lepton identification for $B^0 \to D^{*-}e^+\nu$ events. In this case, the $\mathrm{d}E/\mathrm{d}x$ and E/p selections are loosened, while the requirements on electromagnetic shower shape and Cherenkov angle are removed. This looser selection has efficiency for electrons of approximately 97%, while the pion misidentification probability is about 3%.

3.2 Muon identification

Muon identification relies mainly on the number of measured interaction lengths λ traversed by the track in the IFR iron. At least 2.2λ are required, and at higher momenta we require more than $\lambda_{exp} - 1$, where λ_{exp} is the number of expected interaction lengths as a function of momentum. To reject hadronic showers, we make requirements on the number of hit IFR strips that are parametrized as a function of the penetration length and the distance of the hits from the extrapolated track. In the forward region, which suffers from machine background, extra hit-continuity criteria are applied. In addition, if the particle is in an angular region covered by the EMC, the muon candidate must have an energy deposit in the calorimeter larger than 50 MeV and smaller than 400 MeV.

These same selection criteria are used for both tagging purposes and muon identification in the decay $B^0 \to D^{*-}\mu^+\nu$. The average efficiency and pion misidentification probability are about 75% and 2.5%, respectively.

3.3 Kaon identification

Kaon identification employed for flavor tagging requires the ratio of the combined kaon likelihood to the combined pion likelihood be larger than 15. The combined likelihoods are obtained by multiplying the individual likelihoods from the SVT, DCH and DIRC subsystem information. In the SVT and DCH tracking detectors, the likelihoods are based on the $\mathrm{d}E/\mathrm{d}x$ truncated mean measurement compared to the expected value for the K and π hypotheses, assuming a Gaussian distribution. The $\mathrm{d}E/\mathrm{d}x$ resolution is estimated on a track by track basis given the direction and momentum of the track and the number of energy deposition samples. In the DIRC, the likelihood is computed by combining the likelihoods computed from the measured Cherenkov angle, in comparison with the expected Cherenkov angle for a given mass hypothesis, and the Poisson probability for the observed number of Cherenkov photons, given the number of expected photons for the same hypothesis. DIRC information is not required below 0.7 GeV/c where the DCH $\mathrm{d}E/\mathrm{d}x$ alone provides good K/π discrimination. The efficiency of this selection for kaons is about 85% and the pion misidentification probability is about 5%.

In the reconstruction of B^0 decays, some channels require a very loose kaon selection to reduce backgrounds to acceptable levels. The selection criteria are similar those described above, except that the kaon hypothesis is assumed for those subsystems that have no particle identification information. This looser selection results in a higher kaon efficiency of about 95% and an acceptable pion misidentification probability of 20%. In addition, a loose pion selection is employed in reconstructing some B decay modes. This requirement consists of rejecting pion candidates if they satisfy the tighter kaon or lepton criteria used for flavor tagging described above.

4 Time resolution function

The time difference, $\Delta t = t_{rec} - t_{tag}$, between B decays is determined from the measured separation Δz between the reconstructed B and flavor-tagging decay vertices along the z axis using the known boost, $\Delta t = \Delta z/\beta\gamma c$. The Δt resolution is dominated by the z position resolution for the flavor-tagging B meson vertex. The B_{tag} production point and three-momentum, with its associated error matrix, are derived from the fully reconstructed B_{rec} candidate three momentum, decay vertex and error matrix, and from the knowledge of the average position of the interaction point and the $\Upsilon(4S)$ average boost. These B_{tag} parameters are used as input to a geometrical fit to a single vertex, including all other tracks in the event except those used to reconstruct B_{rec}. In order to reduce bias due to long-lived particles, all possible V^0 candidates that can be reconstructed are used as input to the fit in place of their daughters. Tracks whose contributions to the χ^2 are greater than 6 are removed from the fit, in an iterative procedure that continues until all remaining tracks satisfy this requirement or all tracks are removed.

The time resolution function can be approximated by a sum of three Gaussian distributions with different means and widths

$$\mathcal{R}(\,\Delta t;\,\hat{a}\,) \;=\; \sum_{i=1}^{3} \frac{f_i}{\sigma_i\sqrt{2\pi}} \exp\left(-(\Delta t - \delta_i)^2/2{\sigma_i}^2\right) . \tag{7}$$

Fitting the vertex resolution function with simulated events shows that most of the events ($f_1 = 1 - f_2 - f_3 \approx 70\%$) are found in a core Gaussian component, which has a width $\sigma_1 \approx 0.6$ ps, while the remaining events reside in the tail Gaussian, which has a width $\sigma_2 \approx 1.8$ ps. Tracks from

forward-going charm decays included in the reconstruction of the B_{tag} vertex introduce a small bias, $\delta_1 \approx -0.2\,\mathrm{ps}$, for the core Gaussian towards negative values of Δt.

A small fraction of events have large values of $|\Delta t|$, due to incorrectly reconstructed vertices. This is accounted for in the parameterization of the time resolution function by the third Gaussian component, centered at zero with broad fixed width of 8 ps, making it almost constant over the time interval of the fit. The fraction of events populating this component of the resolution function, $f_w \equiv f_3$ is approximately 2 %.

In the final likelihood fits, we describe the Δt resolution by introducing two scale factors $\mathcal{S}_1$ and $\mathcal{S}_2$ that are applied to the event-by-event resolution, $\sigma_{\Delta t}$, calculated the error on Δz provided by the vertex fit. We take the width of the core and the tail Gaussian components for each event to be $\sigma_1 = \mathcal{S}_1 \times \sigma_{\Delta t}$ and $\sigma_2 = \mathcal{S}_2 \times \sigma_{\Delta t}$, respectively. The scale factor $\mathcal{S}_1$ and the bias δ_1 of the core Gaussian are free parameters in the fit. The scale factor $\mathcal{S}_2$ and the fraction of events in the core Gaussian f_1 are fixed to the values estimated from Monte Carlo simulation by a fit to the pull distribution ($\mathcal{S}_2 = 2.1$ and $f_1 = 0.75$). The bias of the tail Gaussian, δ_2, is fixed at 0 ps. The three free parameters in the likelihood fit are

$$\hat{a} \;=\; \{\,\mathcal{S}_1,\, \delta_1,\, f_w\}\,. \tag{8}$$

We observe no significant differences in simulated events between resolution function parameters obtained from samples involving different decay modes for B_{rec}. This is expected, because Δt resolution is dominated by the precision on the B_{tag}, rather than the B_{rec} vertex. Likewise, the differences in the resolution function parameters for the different tagging categories are also small. Therefore, we use a single set of resolution function parameters $\hat{a}$ for all decay modes. Table 1 shows the values for the vertex parameters obtained in data from a fit to the hadronic B^0 sample, described below.

Table 1: Parameters of the resolution function determined from the sample of events with hadronic fully reconstructed B candidates.

parameter		value	
δ_1	(ps)	-0.20 ± 0.07	from fit
$\mathcal{S}_1$		1.33 ± 0.13	from fit
f_w	(%)	1.6 ± 0.6	from fit
f_1	(%)	75	fixed
δ_2	(ps)	0	fixed
$\mathcal{S}_2$		2.1	fixed

5 Flavor tagging

After the daughter tracks of the reconstructed B are removed, the remaining tracks are analyzed to determine the flavor of the B_{tag}, and this ensemble is assigned a tag flavor, either B^0 or $\overline{B}^0$.

To illustrate the tagging discriminating power of each tagging category, we use as a figure of merit the effective tagging efficiency $Q_i = \epsilon_i \times (1 - 2w_i)^2$, where ϵ_i is the fraction of events associated to the tagging category i and w_i is the mistag fraction, the probability of incorrectly assigning the opposite tag to an event of this category.

We use four different types of flavor tag, or tagging categories, in this analysis. Two of these tagging categories rely upon the presence of a prompt lepton or one or several charged kaons in the event. The remaining two categories, called neural network categories, are based upon the output values of a neural network algorithm applied to all the events that have not already been assigned to one of the `Lepton` or `Kaon` tagging categories.

5.1 Lepton and kaon tags

The `Lepton` and `Kaon` tagging categories use the correlation between the charge of a primary lepton from a semileptonic decay or the charge of a kaon, and the flavor of the decaying b quark. For the `Lepton` category we use both electrons and muons. A minimum center-of-mass momentum requirement on the lepton is applied to reduce the contamination from softer opposite-sign leptons coming from charm semileptonic decays. There are no such discriminating kinematic quantities to reduce the contamination of opposite-sign kaons, so the optimization relies principally on the balance between the kaon identification efficiency and the purity of the kaon sample.

A lepton tag is defined by taking the charge of the fastest identified electron or muon with a center of mass momentum greater than 1.1 GeV/c. A kaon tag is defined by taking the sum of the charges of all identified kaons. If both an electron and a muon are identified, the electron tag takes precedence. If the event has a lepton tag and there is no conflicting kaon tag, the event is assigned to the `Lepton` category. If the event has no lepton tags but has a non-zero kaon tag, the event is assigned to the `Kaon` category. If the event has both lepton and kaon tags but they conflict, the event is not assigned to either the `Lepton` or the `Kaon` category.

5.2 Neural network tags

The use of a second tagging algorithm is motivated by the potential flavor-tagging power carried by non-identified leptons and kaons, softer leptons from charm semileptonic decays, soft pions from D^* decays, and more generally, by the momentum spectrum of charged particles from B meson decays. The best way to exploit the information contained in a set of correlated quantities is to use multivariate methods, such as neural networks, rather than to apply selection cuts.

We design five different neural networks, called subnets, each with a specific goal. Four of the subnets are track-based: the `L` and `LS` subnets are sensitive to the presence of primary and cascade leptons respectively, the `K` subnet to that of charged kaons and the `SoftPi` subnet to that of soft pions from D^* decays. In addition the `Q` subnet exploits the charge of high-momentum particles in the event.

The `L` and `LS` subnets share a set of discriminating kinematic variables in addition to the boolean outputs of the standard lepton identification algorithms. The variables are designed to more fully characterize the kinematic features of a true primary lepton from a semileptonic B decay. Taking all charged tracks in the event, excluding that under consideration as the lepton, together with all neutral clusters we form the recoiling system X. Assuming that B_{tag} is produced at rest in the center-of-mass frame, and that the excluded track is a primary lepton from the B_{tag} semileptonic decay, one can calculate the four-momentum of the neutrino p_ν and the four-momentum p_W of the virtual W boson in the semileptonic decay. The variables available are the center-of-mass momentum of the lepton candidate track, the mass and energy of the recoil system X, the cosine of the angle between the excluded track momentum and the direction of the neutrino, the cosine of the angle between the W momentum direction and the direction of the closest charged or neutral

candidate with energy larger than 50 MeV, and the total energy flow in the hemisphere around the W momentum direction.

The `K` subnet uses the particle momentum in the laboratory frame, together with the three relative likelihoods $L_K/(L_\pi + L_K)$ for the SVT, the DCH and the DIRC.

The `SoftPi` subnet uses the track with the lowest momentum from the B_{tag} decay and the angle it makes with respect to the thrust axis, calculated using all other charged tracks.

The variables of the `Q` subnet are the momentum of the highest momentum track in the B_{tag} system and the sum of momentum-weighted charges normalized by the momentum sum of all tracks with impact parameter less than 1 mm and all neutral clusters with energy greater than 50 MeV.

The variables used as input to the neural network tagger are the highest values of the `L`, `LS` and `SoftPi` subnet outputs each multiplied by the charge of the corresponding tagging track, the highest and the second-highest values of the `K` subnet output again multiplied by the charge of the corresponding tagging tracks, and the output of the `Q` subnet.

The output from the full neural network tagger, x_{NT}, can be mapped onto the interval $[-1, 1]$. The assigned flavor tag is B^0 if x_{NT} is negative, and $\overline{B}^0$ otherwise. Events with $|x_{NT}| > 0.5$ are assigned to the `NT1` tagging category and events with $0.2 < |x_{NT}| < 0.5$ to the `NT2` tagging category. Events with $|x_{NT}| < 0.2$ have very little tagging power and are rejected.

6 Event selection and sample composition

B^0 mesons are reconstructed in the hadronic decay modes $B^0 \to D^{(*)-}\pi^+$, $D^{(*)-}\rho^+$, $D^{(*)-}a_1^+$, $J/\psi K^{*0}$ and the semileptonic decay mode $B^0 \to D^{*-}\ell^+\nu$. All final state particles, with the exception of the neutrino in the semileptonic decay, are reconstructed.

Charged tracks measured by the drift chamber and/or SVT are required to originate within 1.5 cm in xy and 10 cm in z of the nominal beamspot. Electromagnetic clusters in the calorimeter, that are unassociated with charged tracks and used to reconstruct π^0 candidates, are required to have an energy greater than 30 MeV and a shower shape consistent with a photon interaction.

Neutral pion candidates are formed from pairs of electromagnetic clusters assumed to be photons. The invariant mass of the photon pair is required to be within $\pm 20\,\mathrm{MeV}/c^2$ ($2.5\ \sigma$) of the nominal π^0 mass, with a minimum summed energy of 200 MeV. Selected candidates are kinematically fitted with a π^0 mass constraint.

K_S^0 candidates are reconstructed in the $\pi^+\pi^-$ mode, with an invariant mass, computed at the vertex of the two tracks, between 462 and $534\,\mathrm{MeV}/c^2$. The χ^2 of the topological vertex fit is required to have a probability greater than 0.1%. The opening angle between the flight direction and the momentum vector for the K_S^0 candidate is required to be smaller than 200 mr. Finally, the transverse flight distance from the primary vertex in the event, r_{xy}, is required to be greater than 2 mm.

In order to reject "jet-like" events from $e^+e^- \to q\overline{q}$ (continuum) background, we require that the normalized second Fox-Wolfram moment [7] ($R_2 = H_2/H_0$), calculated with both charged tracks and neutral clusters, be less than 0.5 (0.45) in hadronic (semileptonic) decay modes.

6.1 Hadronic B^0 decays

B^0 mesons are reconstructed in the hadronic modes $B^0 \to D^{(*)-}\pi^+$, $B^0 \to D^{(*)-}\rho^+$, $B^0 \to D^{(*)-}a_1^+$ and $B^0 \to J/\psi K^{*0}$. A variety of $\overline{D}^0$, D^-, and D^{*-} modes are used to achieve reasonable efficiency despite the typically small branching fractions for any given B decay channel.

6.1.1 Event selection

We select $\overline{D}^0$, D^- and D^{*-} mesons with the following criteria. $\overline{D}^0$ candidates are identified in the decays channels $K^+\pi^-$, $K^+\pi^-\pi^0$, $K^+\pi^+\pi^-\pi^-$ and $K^0_S\pi^+\pi^-$. D^- candidates are selected using the $K^+\pi^-\pi^-$ and $K^0_S\pi^-$ modes. The D^{*-} candidates are found using the decay $D^{*-} \to \overline{D}^0\pi^-$. Charged and neutral kaons are required to have a momentum greater than 200 MeV/c. The same criterion was applied to the pion in $B^0 \to D^{(*)-}\pi^+$, $B^0 \to D^{(*)-}\rho^+$ decay. For the decay modes $B^0 \to D^{(*)-}a_1^+$, the pions are required to have momentum larger that 150 MeV/c . $\overline{D}^0$ and D^- candidates are required to lie within $\pm 3\sigma$, calculated on an event-per-event basis, of the nominal masses. Pull distributions for the $\overline{D}^0$ and D^- meson masses have been measured in data and were found to have rms in the range of 1.1–1.2 when fitted to a Gaussian form. For $\overline{D}^0 \to K^+\pi^-\pi^0$, we only reconstruct the dominant resonant mode $\overline{D}^0 \to K^+\rho^-$, followed by $\rho^- \to \pi^-\pi^0$. The $\pi^-\pi^0$ mass is required to lie within $\pm 150\,\mathrm{MeV}/c^2$ of the nominal ρ mass and the angle between the π^- and $\overline{D}^0$ in the ρ rest frame, $\theta^*_{D^0\pi}$, must satisfy $|\cos\theta^*_{D^0\pi}| > 0.4$. Finally, all $\overline{D}^0$ and D^- candidates are required to have a momentum greater than 1.3 GeV/c in the $\Upsilon(4S)$ frame and a χ^2 probability of the topological vertex fit greater than 0.1%. A mass constrained fit is applied to candidates satisfying aforementioned requirements and is used in the subsequent reconstruction chain.

We form D^{*-} candidates by combining a $\overline{D}^0$ with a pion which has momentum greater than 70 MeV/c. The soft pion is constrained to originate from the beamspot when the D^{*-} vertex is computed [6]. To account for the small energy release in the decay $\Upsilon(4S) \to B\overline{B}$ (resulting in a small transverse flight of the B candidates), the assumed vertical size of the beam spot is inflated to 40 μm. Monte Carlo simulation was used to verify that this inflation does not introduce any significant bias in the selection or in the Δt measurement. D^{*-} candidates are then required to have $\Delta m = m(\overline{D}^0\pi^-) - m(\overline{D}^0)$ within $\pm 1.1\,\mathrm{MeV}/c^2$ of the nominal value for $\overline{D}^0 \to K^+\pi^-\pi^0$ mode and $\pm 0.8\,\mathrm{MeV}/c^2$ for all the other modes. This corresponds to about $\pm 2.5\sigma$, where the resolution is estimated by taking a weighted average of the core and broad Gaussian components of the observed Δm distributions.

B^0 candidates are formed by combining a D^{*-}, D^- or J/ψ candidate with a π^+, ρ^+, a_1^+ or K^{*0}. For $B^0 \to D^{*-}\rho^+$, the π^0 from the ρ^+ decay is required to have an energy greater than 300 MeV. For $B^0 \to D^{*-}a_1^+$, the a_1^+ is reconstructed by combining three charged pions, with invariant mass in the range 1.0 to 1.6 GeV/c^2. In addition, the χ^2 probability of the vertex fit of the a_1^+ candidate is required to be greater than 0.1%.

As described in Section 3, kaon identification is used to reject background. For most B^0 modes, no identification or only a loose selection is enough to achieve signal purities of 90%. In the $B^0 \to D^-a_1^+$ mode reconstruction, a tight kaon identification is required to alleviate large combinatorial backgrounds.

In order to suppress continuum background, in addition to the R_2 requirement, we calculate the thrust angle, θ_{th}, defined as the angle between the thrust axis of the particles which form the reconstructed B^0 candidate and the thrust axis of the remaining tracks and unmatched clusters in the event, computed in the $\Upsilon(4S)$ frame. The two thrust axes are almost uncorrelated in $B\overline{B}$ events, because the B^0 mesons are almost at rest in the $\Upsilon(4S)$ rest frame. In continuum events, which are more jet-like, the two thrust axes tend to have small opening angles. For final states with a D^* and 2 (3) pions we require $|\cos\theta_{th}| < 0.9$ (0.8) for the $\overline{D}^0 \to K^+\pi^-$ and $K^+\pi^-\pi^0$ modes and 0.8 (0.7) for the $\overline{D}^0 \to K^+\pi^+\pi^-\pi^-$ and $K^0_S\pi^+\pi^-$. No such requirement is applied in the case of the $B^0 \to D^{*-}\pi^+$ mode. In modes which contain a D and a single (2,3) pion(s) in the final state, we require $|\cos\theta_{th}| < 0.9$ (0.8, 0.7).

The $B^0 \to J/\psi K^{*0}$ selection is the same as described in Ref. [8]. The $J/\psi \to e^+e^-$ candi-

dates are formed from pairs of oppositely-charged tracks assumed to be electrons, as explained in Section 3. At least one of the decay products must be positively identified as an electron or, if outside the acceptance of calorimeter, must be consistent with the electron hypothesis from the $\mathrm{d}E/\mathrm{d}x$ measurement in the drift chamber. If both tracks are in the calorimeter acceptance and have a value of E/p larger than 0.5, an algorithm for the recovery of Bremsstrahlung photons [8] is used. The $J/\psi \to \mu^+\mu^-$ candidates are formed from oppositely-charged tracks identified as muons, as described in Section 3. At least one of the decay products must be positively identified as a muon, and the other, if in the acceptance of the calorimeter, must be consistent with a minimum ionizing particle. We retain only those J/ψ candidates with an invariant mass in the range $2.95 < m(J/\psi) < 3.14\,\mathrm{GeV}/c^2$ for the e^+e^- mode and $3.06 < m(J/\psi) < 3.14\,\mathrm{GeV}/c^2$ for the $\mu^+\mu^-$ mode. We reject events with $\cos\theta_{th}$ greater than 0.9.

B^0 candidates are characterized by a pair of nearly uncorrelated kinematic variables, the difference between the energy of the B^0 candidate and the beam energy in the $\Upsilon(4S)$ center-of-mass frame, ΔE, and the beam energy substituted mass, m_{ES} [6]. In the $(m_{\mathrm{ES}}, \Delta E)$ plane the signal region is defined as $5.270 < m_{\mathrm{ES}} < 5.290\,\mathrm{GeV}/c^2$ and $|\Delta E| < 3\sigma_{\Delta E}$. The sideband region is defined as $5.2 < m_{\mathrm{ES}} < 5.26\,\mathrm{GeV}/c^2$ and $|\Delta E| < 3\sigma_{\Delta E}$. The value of $\sigma_{\Delta E}$, the ΔE resolution, is mode-dependent and varies between 19 to 40 MeV. When multiple B^0 candidates (with $m_{\mathrm{ES}} > 5.2\,\mathrm{MeV}/c^2$) are found in the same event, the candidate with the smallest value of $|\Delta E|$ is selected.

6.2 Sample composition

We use the m_{ES} sideband region to measure the combinatorial background fraction, to characterize the background Δt distribution, and to measure the fraction of mixed events contributed from background under the B^0 signal peak. It is therefore useful to check that the background composition in the m_{ES} sideband region is similar to that in the signal region. The validity of this background estimation procedure was checked on 2.0 fb^{-1} of simulated data. We also compared the m_{ES} sideband shape in data with the Monte Carlo and found good agreement.

The B^0 signal yield and sample purity extracted from fits to the m_{ES} distribution are summarized in Table 2. The net B^0 signal sample, before applying any decay vertex requirements, consists of 2577 ± 59 signal candidates with a purity of about 86%.

Table 2: Two-body hadronic B^0 decay candidate yields and signal purities from the fit to the m_{ES} distribution. Signal purities are estimated for $m_{\mathrm{ES}} > 5.27\,\mathrm{GeV}/c^2$.

Decay mode	Number of B^0 candidates	S/(S+B) [%]
$B^0 \to D^{*-}\pi^+$	622 ± 27	90
$B^0 \to D^{*-}\rho^+$	419 ± 25	84
$B^0 \to D^{*-}a_1^+$	239 ± 19	79
$B^0 \to D^-\pi^+$	630 ± 26	90
$B^0 \to D^-\rho^+$	315 ± 20	84
$B^0 \to D^-a_1^+$	225 ± 20	74
$B^0 \to J/\psi\, K^{*0}$	194 ± 15	90
Total	2577 ± 59	86

In order to select B^0 candidates with well understood B decay vertex error, we require the

convergence of the topological fit for B^0 decay vertex. B^0 candidates with $|\Delta z| > 3.0\,\mathrm{mm}$ or with $\sigma_{\Delta z} > 400\,\mu\mathrm{m}$ are removed.

The efficiency for each tagging category is calculated as the number of signal events for each tag, divided by the total number of signal events after vertex cuts are imposed. The tagging efficiency and signal purity for the individual tagging categories in data are extracted from fits to the m_{ES} distributions shown in Fig. 1 and are listed in Table 3. The distributions are fitted with a Gaussian distribution for the signal and the ARGUS background function for the background parametrization [9]. All fits have good confidence levels.

Table 3: Tagging efficiencies for hadronic B^0 decays and signal purities in data separately for the four tagging categories. Signal purities are estimated for $m_{\mathrm{ES}} > 5.27\,\mathrm{GeV}/c^2$.

Tagging Category	Efficiency [%]	B candidates	S/(S+B) [%]
`Lepton`	10.5 ± 0.6	260 ± 17	95
`Kaon`	36.7 ± 1.0	918 ± 34	86
`NT1`	12.0 ± 0.7	305 ± 19	89
`NT2`	16.4 ± 0.7	405 ± 24	81
All tags	75.6 ± 0.9	1886 ± 49	87

6.3 Semileptonic B decays

The semileptonic decay $B^0 \to D^{*-}\ell^+\nu$, with a measured branching fraction of $4.6 \pm 0.27\%$ [3], is a copious source of B^0 mesons. We reconstruct the D^{*-} through its decay to $\overline{D}^0\pi^-$, and use the three $\overline{D}^0$ decay modes $K^+\pi^-$, $K^+\pi^+\pi^-\pi^-$ and $K^+\pi^-\pi^0$.

6.3.1 Event selection

We reconstruct $\bar{D}^0$ candidates in the three modes listed above. All reconstructed $\bar{D}^0$ candidates are required to have an invariant mass within $\pm 2.5\sigma$ of the nominal D^0 mass. The $\bar{D}^0$ topological vertex fit is required to have a χ^2 probability greater than 1%; for the $\bar{D}^0 \to K^+\pi^-\pi^0$ mode this vertex fit includes a kinematic constraint on the π^0 mass. There are no additional requirements for $\bar{D}^0 \to K^+\pi^-$. For $\bar{D}^0 \to K^+\pi^+\pi^-\pi^-$ and $\bar{D}^0 \to K^+\pi^-\pi^0$ we require loose K and π particle identification as described in Section 3, and a minimum π^0 momentum of $200\,\mathrm{MeV}/c$. In addition, the K and π candidates are required to have momenta greater than 200 and $150\,\mathrm{MeV}/c$, respectively, for the mode $\bar{D}^0 \to K^+\pi^+\pi^-\pi^-$. The decay $\bar{D}^0 \to K^+\pi^-\pi^0$ occurs mostly through resonant substructures. The ρ and K^* resonances dominate and we use the measured Dalitz weights to construct an event-by-event probability and select events using this quantity to suppress combinatorial background[2].

$\bar{D}^0$ candidates satisfying the above requirements are combined with all charged tracks, having a minimum transverse momentum of $50\,\mathrm{MeV}/c$ and charge opposite to that of the candidate kaon, to form D^* candidates. The mass difference $m(D^{*-}) - m(\bar{D}^0)$ is calculated and required to lie within 2.5σ of the nominal value.

Finally, D^* candidates are combined with electron or muon candidates, with momentum greater than $1.2\,\mathrm{GeV}/c$ and satisfying the lepton identification requirements described in Section 3. The

[2]The Dalitz weights are used in the time-integrated analysis. The time-dependent analysis uses the $\bar{D}^0 \to K^+\rho^-$ sample only.

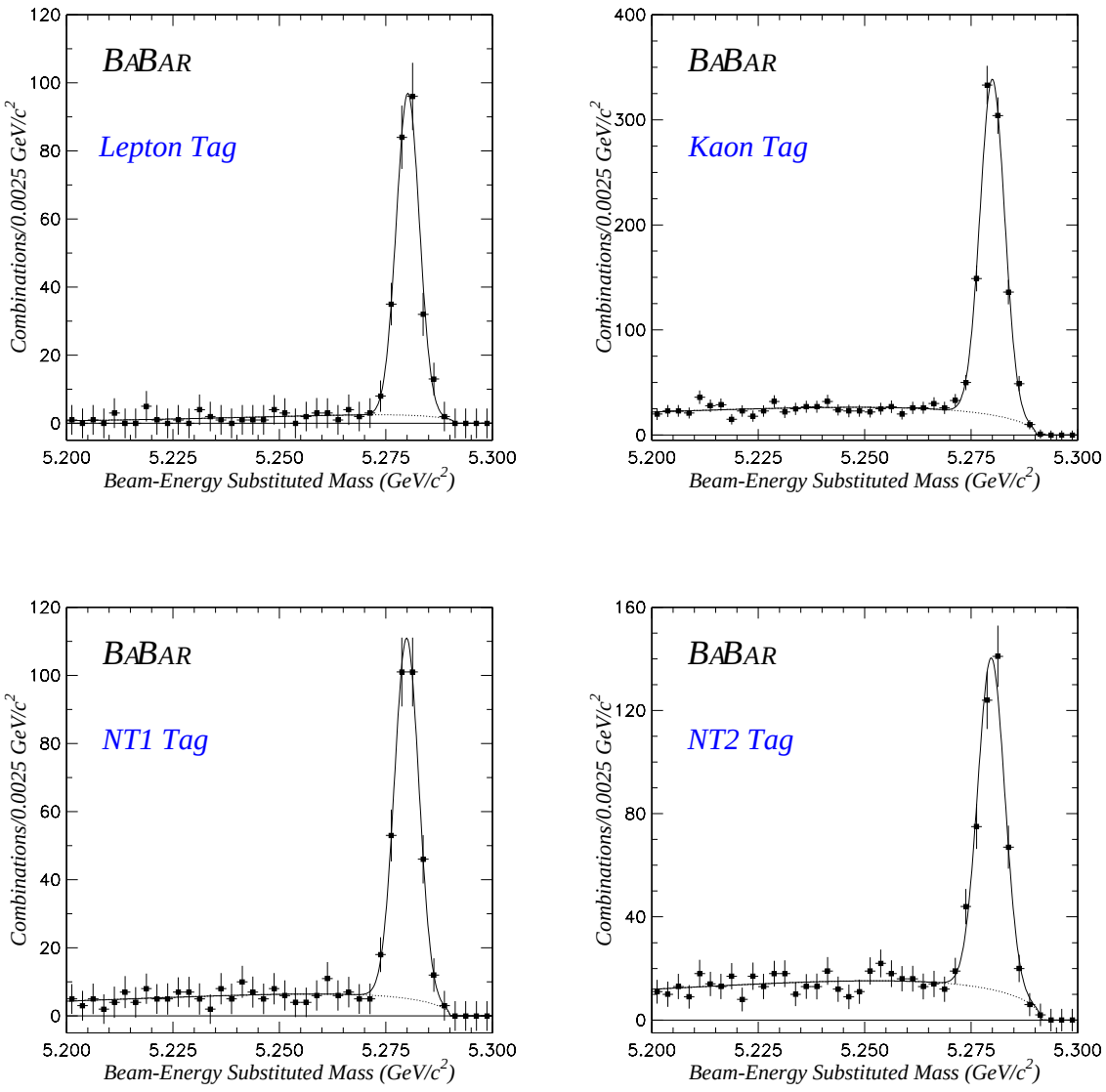

Figure 1: $m_{\rm ES}$ distribution for each tagging category (`Lepton`, `Kaon`, `NT1` and `NT2`) for all the hadronic B^0 modes.

D^* – lepton topological vertex fit is required to have a χ^2 probability greater than 1%, and the lepton and D^* candidates must have opposite charge. The D^* and lepton tend to be back-to-back in the B^0 rest frame, so we require $\cos\theta(D^* - l) < 0$ where $\theta(D^* - l)$ is the angle between the D^* and the lepton in the center-of-mass frame.

The neutrino cannot be reconstructed, but we require that the candidate four-momenta be consistent with a missing particle of zero mass:

$$(p_B - p_{D^*} - p_l)^2 = p_\nu^2 = 0. \tag{9}$$

Solving this equation in the $\Upsilon(4S)$ frame, we obtain a constraint on the angle between the B^0 and the $D^* - l$ system:

$$\cos\theta(B, D^*l) = \frac{M_B^2 + M_{D^*l}^2 - 2E_B E_{D^*l}}{2|\vec{p}_B||\vec{p}_{D*l}|}. \tag{10}$$

Only the mass and scalar momentum of the initial state B^0, both of which are known, is required to calculate the angle $\theta(B, D^*l)$ and not the flight direction. In $B^0 \to D^*l\nu$ decay, the cosine of this angle must lie in the region $(-1, +1)$. Allowing for detector resolution effects in the reconstructed momenta and angles, we require $|\cos\theta(B - D^*l)| < 1.1$.

After applying these criteria, we obtain a sample of 7517 ± 104 $B \to D^*l\nu$ events: 3101 ± 64 in the $\bar{D}^0 \to K^+\pi^-$ mode, 1986 ± 51 in the $\bar{D}^0 \to K^+\pi^-\pi^0$ mode, and 2430 ± 56 in the $\bar{D}^0 \to K^+\pi^+\pi^-\pi^-$ mode.

6.3.2 Sample composition

The events are flavor tagged as described in Section 5. The $D^* - D^0$ mass difference distributions for each tagging category are shown in Fig. 2. The backgrounds are evaluated separately for each tag category. Backgrounds are larger for the semileptonic modes than for the hadronic modes and originate from a variety of sources. Each source of background is evaluated using a control sample that is taken from data whenever possible. The background control samples are used to measure the background fractions, to characterize the background Δt distribution, and to measure the fraction of mixed events contributed by each source of background.

We divide the backgrounds to $B^0 \to D^*l\nu$ into three types: events with an incorrectly reconstructed D^* ("combinatorial" background), events in which a true D^* is combined with an incorrect lepton candidate ("wrong-lepton" background), and events in which a correctly identified D^*-lepton pair originates from semileptonic B^+ decay, for example from the decay $B^+ \to \bar{D}^{**0}l^+\nu$, followed by $\bar{D}^{**0} \to D^{*-}n\pi^+$ ("B^+ background"). The symbol $\bar{D}^{**0}$ refers to an admixture of orbitally or radially excited charmed meson resonances which decay via strong interaction into a D^{*-}. Events of the type $B^0 \to D^{**-}l^+\nu$ are considered as signal.

Combinatorial background

The fraction of combinatorial background, due to falsely reconstructed D^* candidates, is estimated by fitting the $\Delta m(D^* - D^0)$ distributions. We use a Gaussian distribution to characterize the signal and a threshold function with a sharp rise followed by an exponential tailoff to characterize the background shape. the signal region is defined to lie within $\pm 2.5\sigma$ of the peak in $\Delta m(D^* - D^0)$, while events in the the sideband region $0.150 < \Delta m(D^* - D^0) < 0.160\,\mathrm{GeV}/c^2$ provide the combinatorial background control sample.

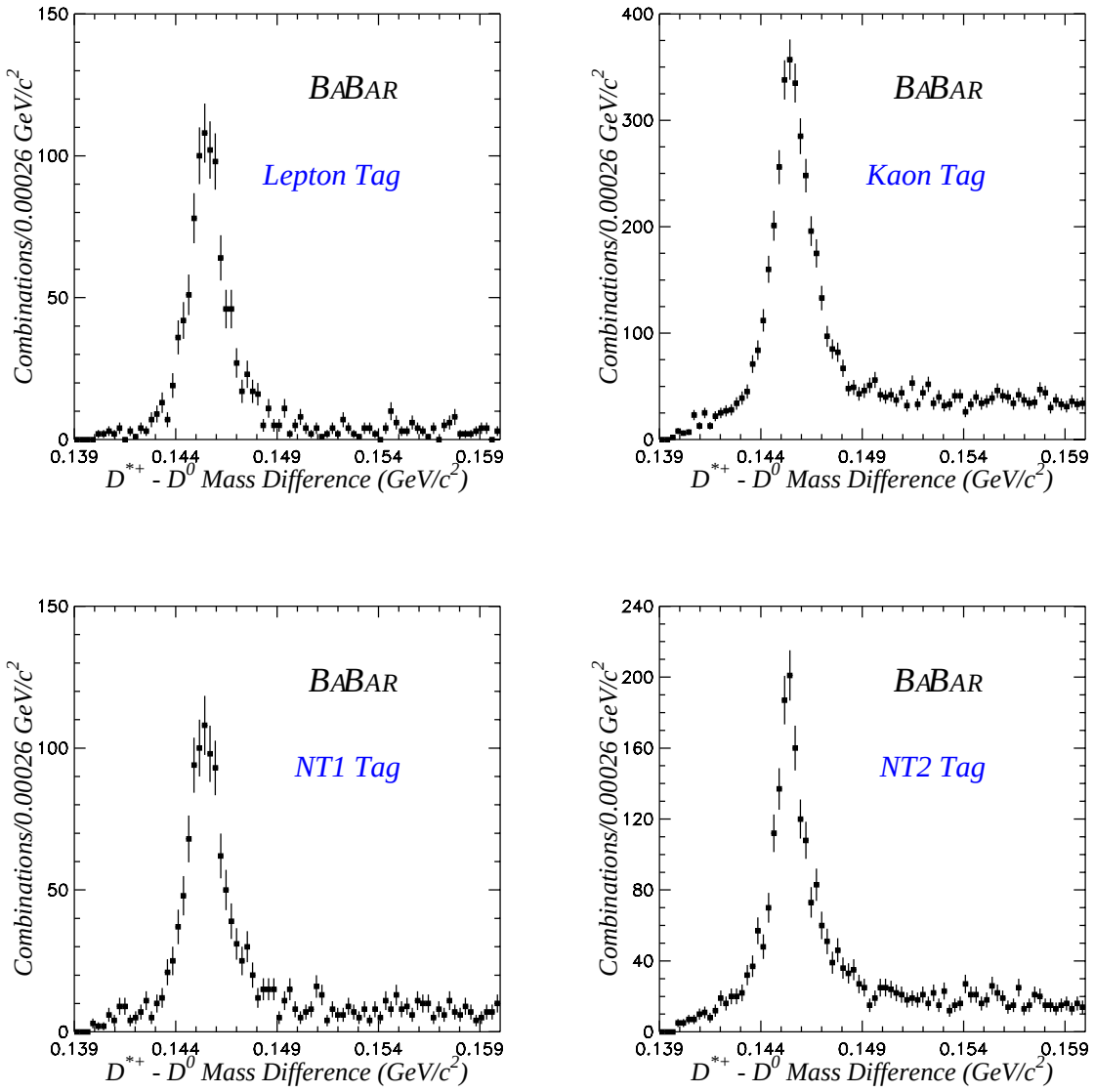

Figure 2: $D^* - D^0$ mass difference distribution for each tagging category (`Lepton`, `Kaon`, `NT1` and `NT2`) for the $D^* l\nu$ sample.

Wrong-lepton background

There are four potential sources of background events in which a real D^* is combined with a wrong lepton. We consider each in turn.

First, there are events in which the lepton candidate is not a real lepton, but is misidentified as such. This "fake lepton" background is estimated from data by selecting events in which a track candidate that has failed very loose lepton criteria is substituted for the lepton candidate. These events are weighted with the lepton mis-identification probabilities measured in data to estimate the fraction of fake lepton background, after subtraction of the combinatorial background contribution.

The second type of wrong lepton events is due to a real D^* from one B combined with a real lepton from the other B. These "uncorrelated lepton" backgrounds are due to $B^0\overline{B}^0$ events where mixing has occurred, yielding the right D^*l sign combination, or events in which a lepton originating from a secondary charm decay is combined with a D^* from the other B. The D^* and lepton directions are uncorrelated in these events, prior to application of the $\cos\theta(D^*l)$ and $\cos\theta(B-D^*l)$ selection criteria.

To estimate this background from data, the lepton momentum vector in the $\Upsilon(4S)$ center-of-mass frame is parity-inverted, prior to the calculation of the $\theta(D^*-l)$ and $\theta(B-D^*l)$. Events with a correlated back-to-back D^*-l pair fail these criteria after the lepton momentum is flipped, but events with a randomly correlated D^*-l pair pass with approximately the same efficiency as in the original sample. After removing the remaining signal contribution, and correcting for residual combinatorial background, we estimate the uncorrelated lepton background from the flipped-lepton control sample.

Third, there are decays of the type $B^0 \to D^*DX$, where the D decays semileptonically producing a non-primary lepton. The momentum requirement on the lepton rejects most of these "cascade lepton" events; the remaining fraction, estimated from Monte Carlo simulation, is less than 1% and has been neglected.

Finally, $c\bar{c}$ events can produce a real D^* and a real lepton in a back-to-back configuration. The $c\bar{c}$ background fraction has been estimated using combinatorial-subtracted off-resonance data. We use the off-resonance data as a control sample to characterize the Δt distribution and the mixed event contribution from this background source.

B^+ background

In addition to the well-studied semileptonic decays $B \to Dl\nu$ and $B \to D^*l\nu$, a significant fraction of B semileptonic decays involve additional final state particles, either produced through D^{**} resonances or non-resonantly. These processes of the type $B \to D^*(n\pi)l\nu$ contribute to both the neutral and charged semileptonic B decays.

For the purposes of this analysis, neutral semileptonic decays $B^0 \to D^*(n\pi)l\nu$ that pass our event selection criteria are considered to be part of the signal. They contribute equally to the measurement of Δm_d, and the additional low-momentum pion does not affect the tagging algorithm.

However, the charged B decays of the type $B^- \to D^{*+}(n\pi)l^-\nu$ are considered as background for this analysis. They do not oscillate and must be corrected for in extracting Δm_d; their mistag rate may differ from that of B^0 decays as well.

We assume a lifetime and Δt resolution for charged B events that is the same as that for the B^0 signal events. The mistag rate is estimated directly from data using fully reconstructed B^+ decays. It is difficult to accurately estimate the fraction of this background, since it cannot be cleanly separating from the signal. To estimate the fraction of events due to charged B decay,

Table 4: Sample composition and yields in tagged $B^0 \to D^* l\nu$ events

	Lepton	Kaon	NT1	NT2
Combinatorial	0.063±0.008	0.161±0.007	0.128±0.011	0.158±0.009
Fake Lepton	0.032±0.007	0.035±0.007	0.031±0.007	0.030±0.007
Uncorr. Lepton	0.015±0.016	0.035±0.012	0.024±0.013	0.028±0.013
$c\bar{c}$	0.000±0.007	0.026±0.010	0.025±0.017	0.056±0.021
$B^{\pm}$	0.062±0.040	0.052±0.031	0.055±0.038	0.051±0.034
Signal Fraction	0.827±0.040	0.691±0.031	0.737±0.038	0.677±0.034
Tagged Event Yield	863 ±32	2804 ±63	850 ±34	1318 ±43
Tag Efficiency	0.121 ±0.007	0.368 ±0.017	0.114 ±0.006	0.169 ±0.009

we rely on an estimate of their production rate, combined with a Monte Carlo study of the event selection efficiency for these modes.

The inclusive branching fraction, $\mathcal{B}(B^+ \to D^{*-}(n\pi)l^+\nu) = 1.25\pm0.16\%$ is taken from LEP measurements [10]. We use Monte Carlo simulation to study the efficiency of the event selection criteria for events of this type, averaging over several resonant D^{**} and non-resonant states. The average efficiency is found to be $4.25\pm 3.0\%$, where a conservative systematic error has been assigned due to the lack of knowledge of the relative decay fractions for the possible modes. The product of the branching ratio times the event selection efficiency, $\mathcal{B}\times\epsilon(B^+)$, and the corresponding product $\mathcal{B}\times\epsilon(B^0)$ for the neutral B signal events are computed, where decays of the type $\overline{B}^0 \to D^{*+}(n\pi)l^-\nu$ are included as part of the signal. By this method, we find:

$$f(B^+) = \frac{\mathcal{B}*\epsilon(B^+)}{\mathcal{B}*\epsilon(B^+)+\mathcal{B}*\epsilon(B^0)} = 7.1\pm\ 5.0\% \tag{11}$$

Background summary

The background contributions in $B \to D^* l\nu$ events, averaged over D^0 decay modes, are summarized by tag category in Table 4.

7 Likelihood fit method

In the presence of backgrounds, the probability distribution functions $\mathcal{H}_{\pm}$ of Eq. 3 must be extended to include a term for each significant background source. The background parameterizations are allowed to differ for each tag category. Each event is identified as being either mixed $(-)$ or unmixed $(+)$ and as belonging to a particular tag category, i. Thus a distribution must be specified for each possibility $(+/-, i)$:

$$\mathcal{H}_{\pm,i} = f_{sig,i}\mathcal{H}_{\pm}(\Delta t;\Gamma,\Delta m_D,\mathcal{D}_i,\hat{a}_i) + \sum_{\beta=\text{bkgd}} f_{\beta,i}\mathcal{B}_{\pm,i,\beta}(\Delta t;\hat{b}_{\pm,i,\beta}) \tag{12}$$

where the background PDFs, $\mathcal{B}_{\pm,i,\beta}$, provide an empirical description the Δt distribution of the background events in the sample. The fraction of background events for each source and tagging category is given by $f_{\beta,i}$, while $\hat{b}_{\pm,i,\beta}$ are parameters used to characterize each source of background

by tagging category for mixed and unmixed events. The signal fraction in each tag category is given by

$$f_{sig,i} = 1 - \sum_{\beta} f_{\beta,i} \tag{13}$$

The distributions are normalized so that for each i and β

$$\int_{-\infty}^{\infty} d\Delta t(\mathcal{B}_{+,i,\beta} + \mathcal{B}_{-,i,\beta}) = 1. \tag{14}$$

7.1 Background parameterization

Backgrounds stem from many different sources; we use control samples, derived whenever possible from the data itself, to characterize the background time dependence and dilution. These control samples were described in Section 6. We use an empirical description for the time dependence of the backgrounds in the likelihood fit allowing for three time components for each background, each with its own dilution factor $\mathcal{D}$ and a common resolution function $\mathcal{R}$:

- Zero lifetime component: $B_{\pm,1} = (1 \pm \mathcal{D}'_1)\delta(t) \otimes \mathcal{R}$
- Non-zero lifetime component, no mixing: $B_{\pm,2} = \frac{\Gamma_2}{2}(1 \pm \mathcal{D}'_2)\ \mathrm{e}^{(-\Gamma_2|\Delta t|)} \otimes \mathcal{R}$
- Non-zero lifetime component, with mixing: $B_{\pm,3} = \frac{\Gamma_3}{2}\mathrm{e}^{(-\Gamma_3|\Delta t|)}(1 \pm \mathcal{D}_3 \cos(\Delta m_3 \Delta t)) \otimes \mathcal{R}$

A likelihood fit to the background control samples is used to determine how much of each time component is present and to fit for the apparent lifetimes, resolution, mixing and dilutions that best describe the background sample. This approach allows for more fit parameters than are absolutely necessary. The goal is to determine the background shapes as well as possible in an empirical sense.

7.2 Likelihood fit results

7.2.1 Hadronic decay modes

We extract Δm_d and the mistag rates by fitting the Δt distributions of the selected B candidate events with $m_{\rm ES} > 5.2\,\mathrm{GeV}/c^2$ with the likelihood function described above. The probability that a B candidate is a signal or a background event is determined from a fit to the $m_{\rm ES}$ distribution. We describe the $m_{\rm ES}$ shape with a single Gaussian $S(m_{\rm ES})$ for the signal and the ARGUS function [9] $B(m_{\rm ES})$ for the background. Based on this fit, the event-by-event signal probability is determined from:

$$p_{\rm sig}(m_{\rm ES}) = \frac{S(m_{\rm ES})}{S(m_{\rm ES}) + B(m_{\rm ES})} \tag{15}$$

The contribution of each event to the fitted signal parameters corresponds to this signal probability.

The Δt distributions of the combinatorial background are described with a zero lifetime component and a non-oscillatory component with non-zero lifetime. We fit for separate resolution function parameters for the signal and the background in order to minimize correlations between the background parameters and the signal parameters.

We use the data sample described in Section 6, consisting of $\approx$ 1900 fully-reconstructed and tagged B^0 candidates. The Δt distributions of those candidates, overlaid with the likelihood fit results, are shown in Fig. 3 for the candidates with $m_{\rm ES} > 5.27\,\mathrm{GeV}/c^2$. The Δt distributions

for the background candidates in data from the $m_{\rm ES}$ sideband ($m_{\rm ES} < 5.27\,{\rm GeV}/c^2$) are shown in Fig. 4. In Fig. 5 the mixing asymmetry of Eq. 2 is plotted; the primordial cosine function is clearly visible. The results from the likelihood fit to data are summarized in Table 5. The tagging separation $Q = \epsilon_{tag}(1-2w)^2$ is calculated from the mistag rate and the efficiency quoted in Table 3. Summing over all tagging categories, we measure a combined effective tagging efficiency $Q \approx 28\%$.

Table 5: Results from the likelihood fit to the Δt distributions of the hadronic and semileptonic B decays. Δm_d and the mistag rates include small corrections corresponding to the difference between the generated and reconstructed values in simulated signal events. The summed Q over all tagging catagories is 0.285 (0.283) for hadronic (semileptonic) decay modes.

Parameter	Hadronic		Semileptonic	
	Fit Value	$Q = \epsilon(1-2w)^2$	Fit Value	$Q = \epsilon(1-2w)^2$
Δm_d [$\hbar$ ps^{-1}]	0.516 ± 0.031	—	0.508 ± 0.020	—
w(Lepton)	0.116 ± 0.032	0.062	0.084 ± 0.020	0.071
w(Kaon)	0.196 ± 0.021	0.136	0.199 ± 0.016	0.133
w(NT1)	0.135 ± 0.035	0.064	0.210 ± 0.028	0.066
w(NT2)	0.314 ± 0.037	0.023	0.361 ± 0.025	0.013
scale$_{\rm core,\ sig}$	1.33 ± 0.13	—	1.32 ± 0.07	—
$\delta_{\rm core,\ sig}$ [ps]	–0.20 ± 0.07	—	–0.25 ± 0.04	—
$f_{\rm outlier}$	0.016 ± 0.006	—	0.000 ± 0.002	—

As a validation of these results we have carried out identical analysis procedures on simulated Monte Carlo events generated with a detailed detector simulation, processed through the event reconstruction chain in the same manner as the data. In the signal simulation, the fitted values of the $B^0\overline{B}^0$ oscillation frequency, $\Delta m_d = 0.451\pm\ 0.011\ \hbar\,{\rm ps}^{-1}$ (hadronic decays) and $\Delta m_d = 0.456\pm\ 0.009\ \hbar\,{\rm ps}^{-1}$ (semileptonic decays), are consistent with the value of 0.464 $\hbar\,{\rm ps}^{-1}$ used for Monte Carlo generation. The fitted tagging dilutions and mistag rates are in good agreement with the values obtained from Monte Carlo truth information, confirming an unbiased measurement of those parameters. We apply the observed differences as a correction to the measured values in data, although all parameters as determined from the simulated sample are consistent with the generated values.

7.2.2 Semileptonic decays

The event selection for the $B \to D^* l\nu$ sample is summarized in Section 6. The yield of tagged $B \to D^* l\nu$ events and the signal purity are described in Section 6.

The measurement of $B^0\overline{B}^0$ mixing and the extraction of Δm_d and the mistag fractions with $B \to D^* l\nu$ decays proceeds in two steps. First, we fit the background control samples described in Section 6 and determine their parameters.

Second, we fit the signal events, fixing the background fractions to the values summarized in Table 4 and the Δt resolutions and dilution parameters to the values obtained from fits to the control samples. The results of the fit and the calculated tagging performance, $Q = \epsilon_{tag}(1-2w)^2$, are summarized in Table 5. The Δt distribution of the $B \to D^* l\nu$ candidates, overlaid with the likelihood fit result, is shown in Fig. 6

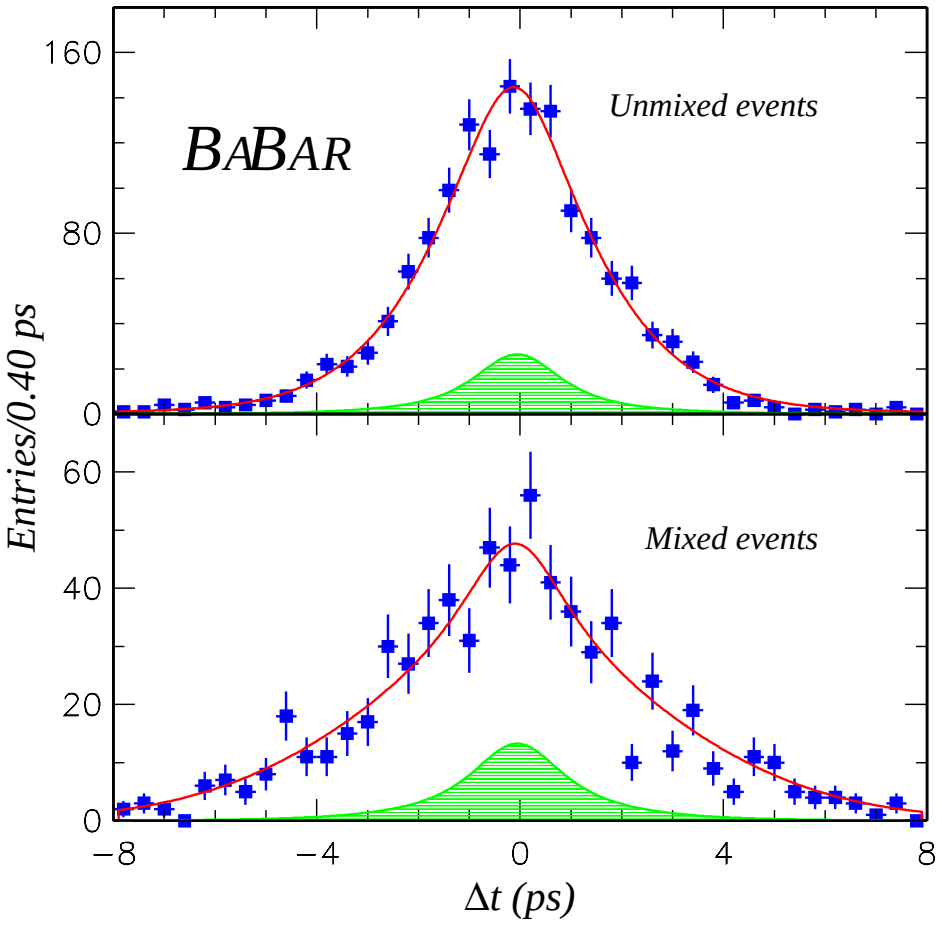

Figure 3: Δt distributions in data for the signal hadronic B sample with $m_{\rm ES} > 5.27\,{\rm GeV}/c^2$. The fitted Δt shapes for the selected candidates and for the fraction of background candidates are overlaid. The confidence level for this projection of the fit result is calculated from the binned Δt distributions using a Poisson-χ^2 technique to be 13% .

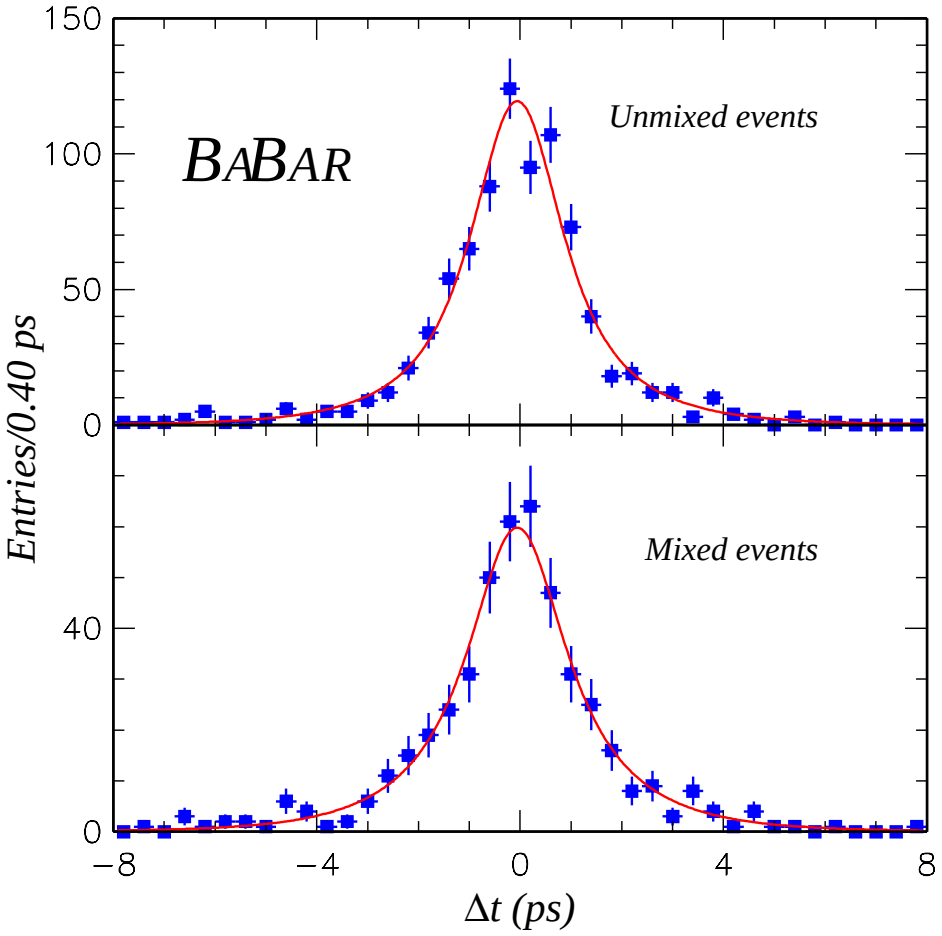

Figure 4: Δt distributions in data for the background candidates with $m_{\rm ES} < 5.27\,{\rm GeV}/c^2$ separately for unmixed and mixed candidates. The fitted Δt shapes for those candidates are overlaid. The confidence level for this projection of the fit result is calculated from the binned Δt distributions using a Poisson-χ^2 technique to be 21% .

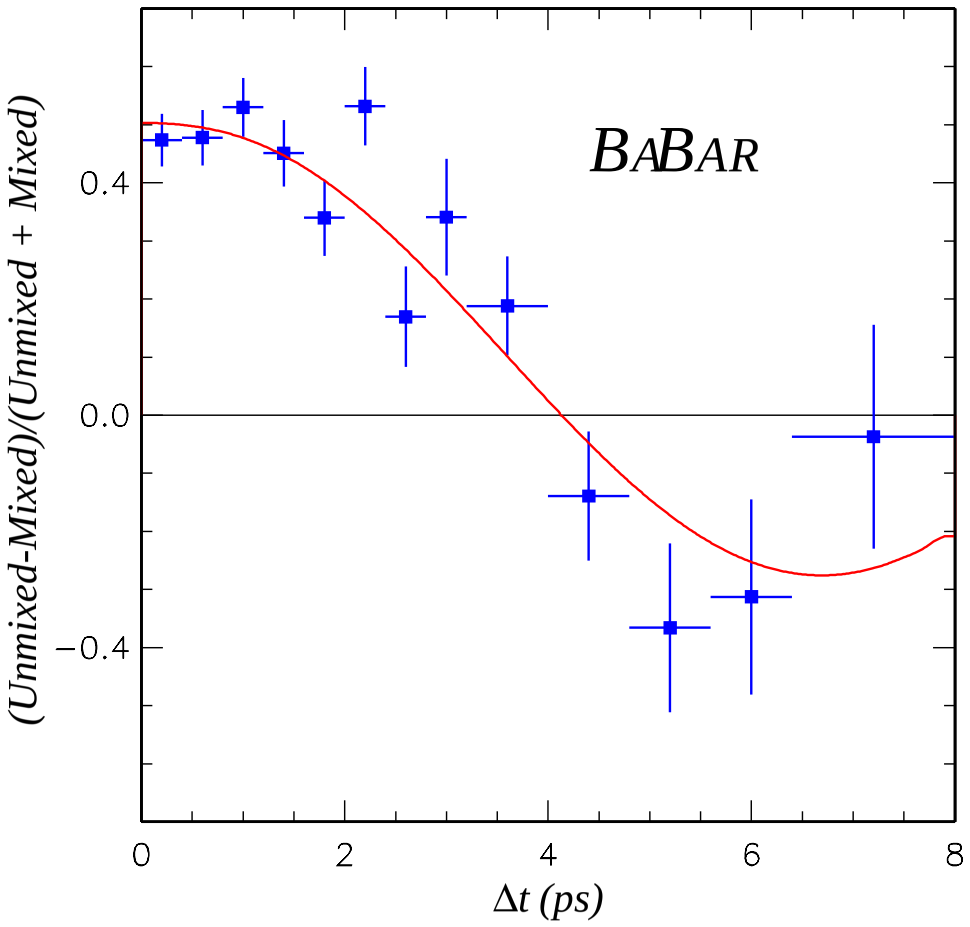

Figure 5: Time-dependent asymmetry $a(\Delta t)$ between unmixed and mixed events for hadronic B candidates with $m_{\rm ES} > 5.27\,{\rm GeV}/c^2$.

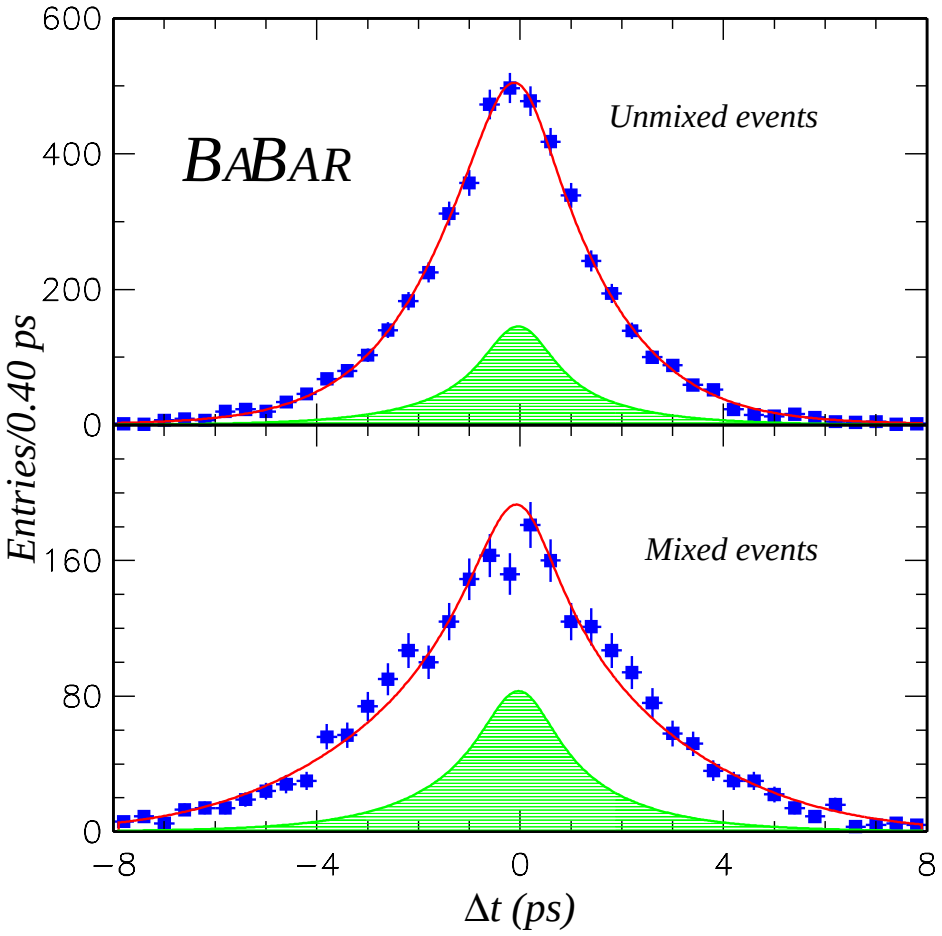

Figure 6: Δt distributions in data for the selected $B \to D^* l\nu$ candidates for unmixed and mixed candidates. The fitted Δt shapes for those candidates and for the fraction of background candidates are overlaid. The confidence level for this projection of the fit result is calculated from the binned Δt distributions using a Poisson-χ^2 technique to be 28%.

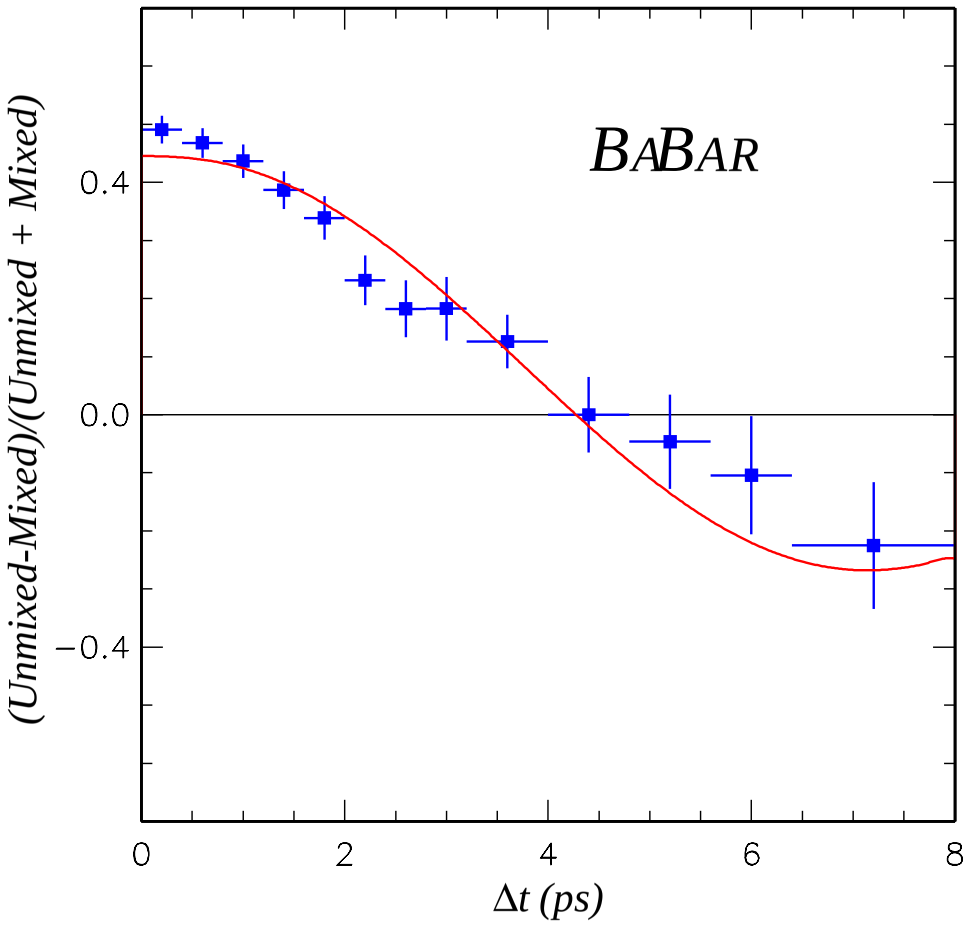

Figure 7: Time-dependent asymmetry between unmixed and mixed events for $B \to D^* l\nu$ candidates.

7.3 Systematic error estimation

The systematic errors for the hadronic and semileptonic B samples are summarized in Tables 6 and 7 and can be grouped into three categories:

Δt reconstruction

We determine the level of any potential systematic bias in Δm_d and the mistag rates due to the Δt resolution function by independently varying the scale factor and the mean of the wide Gaussian and the fraction of events in the wide Gaussian. The variations correspond to a change in the RMS of the total resolution function by one standard deviation as measured in data. The systematic uncertainty due to Δt outliers is estimated from the variation of the fitted parameters with the fraction of outliers and the RMS of their Δt distribution in a sample of toy Monte Carlo events. An error in the boost of the $\Upsilon(4S)$ system or in the z scale of the detector can bias the Δm_d measurement because those parameters are used to reconstruct a decay length difference Δz and to convert it to the decay time difference Δt. In the likelihood fit, we fix the B^0 lifetime to the PDG value [3] and its uncertainty leads to a systematic error.

Background parameters

The signal probability assigned to each candidate in the hadronic B sample has a statistical uncertainty, and these statistical uncertainties lead to systematic uncertainties in Δm_d and the mistag rates. We estimate these uncertainties by varying the width and height of the fitted peak in $m_{\rm ES}$ by one standard deviation.

In the semileptonic sample we vary the average background fractions by the statistical uncertainties derived from the control samples. The uncertainty in the fraction of $D^*\ell\nu$ candidates with a fake lepton includes the uncertainty in the lepton identification rates. To estimate the sensitivity of Δm_d and the mistag rates to the Δt description of the combinatorial background, we repeat the likelihood fit with an additional oscillatory term in the PDF. In the fit to the signal sample we vary the background dilutions obtained from the control samples by one standard deviation. We study the sensitivity to the resolution function of the combinatorial backgrounds by allowing an additional scale factor to account for possible tails in the Δt distribution.

Check with simulated events

Candidate selection criteria can cause systematic biases in the measurement of Δm_d and the mistag rates. These biases are estimated with fully simulated events and are found to be consistent with zero within their statistical uncertainty. Nevertheless, we correct for the actual differences between the generated and reconstructed values and include the statistical uncertainties in the measured parameters from the simulated events as a contribution to the systematic uncertainties in the result.

8 Time-integrated method

8.1 Description of the method

As previously described in Section 1, a time-integrated method to measure the mistag fractions in data provides a simple and robust check of the likelihood fit method presented in Section 7. The statistical precision of this method is enhanced by restricting the sample to events in a single

Table 6: Systematic uncertainties for Δm_d and the mistag rates measured with hadronic B decays for the likelihood fit.

Source	Δm_d $[\hbar\ \mathrm{ps}^{-1}]$	Lepton	Kaon	NT1	NT2
Δt Resolution	0.011	0.004	0.004	0.004	0.004
Background Δt	0.002	0.002	0.002	0.002	0.002
Background Resolution	0.002	0.002	0.002	0.002	0.002
Background Fractions	0.004	0.004	0.002	0.006	0.004
B^0 lifetime	0.005	0.001	0.001	0.001	0.001
z scale	0.005	—	—	—	—
z boost	0.003	—	—	—	—
Monte Carlo Correction	+0.013 ± 0.011	–0.001 ± 0.011	0.000 ± 0.008	–0.010 ± 0.015	–0.015 ± 0.014
Total Systematic Error	0.018	0.013	0.010	0.017	0.015
Statistical Error	0.031	0.032	0.021	0.035	0.037
Total Error	0.036	0.035	0.023	0.039	0.040

Table 7: Systematic uncertainties in Δm_d and in the mistag rates measured with semileptonic B decays for the likelihood fit.

Source	Δm_d $[\hbar\ \mathrm{ps}^{-1}]$	Lepton	Kaon	NT1	NT2
Δt Resolution	0.012	0.005	0.009	0.012	0.005
Background Δt	0.002	0.002	0.002	0.002	0.002
Background Resolution	0.002	0.002	0.002	0.002	0.002
Background Dilutions	0.006	0.008	0.013	0.026	0.031
Background Fractions	0.006	0.009	0.011	0.017	0.032
B^+ Backgrounds	0.010	0.009	0.010	0.004	0.003
B^0 lifetime	0.006	0.001	0.001	0.001	0.001
z scale	0.005	—	—	—	—
z boost	0.003	—	—	—	—
Monte Carlo Correction	+0.008 ± 0.009	–0.010 ± 0.008	–0.001 ± 0.006	–0.002 ± 0.011	–0.006 ± 0.011
Total Systematic Error	0.022	0.018	0.023	0.035	0.046
Statistical Error	0.020	0.020	0.016	0.028	0.025
Total Error	0.030	0.027	0.031	0.045	0.052

optimized Δt interval. Taking into account the *BABAR* vertex resolution, the optimum interval is found to be $|\Delta t| < 2.5\,\text{ps}$. This is so because the number of mixed events in this time interval is dominated by the mistag rate rather than by $B^0\overline{B}^0$ mixing. Events with $|\Delta t| > 2.5\,\text{ps}$ have on average equal numbers of mixed and unmixed events due to $B^0\overline{B}^0$ oscillations, and therefore contribute nothing to the determination of the mistag rate. We refer to this time-integrated method using a single optimized Δt interval as the "single-bin" method.

The single-bin analysis uses the reconstructed hadronic and semileptonic B^0 sample described in Section 6. The number of tagged events in each category were summarized in Table 3 and Table 4. The background fractions were re-evaluated for the sample of tagged signal events with $|\Delta t| < 2.5\,\text{ps}$.

To correct for the presence of backgrounds, we must add to Equation 6 a term to account for the contribution of each background source to the fraction of mixed events in the sample:

$$\chi_{obs} = f_s(\chi_d + (1 - 2\chi_d)\, w) + \sum_\beta f_\beta \chi_\beta, \tag{16}$$

where f_s, f_β are the fraction of signal and each background source, respectively, χ_β is the fraction of mixed events in each background source, and χ_{obs} is the observed fraction of mixed events. We restrict the sample to events with $|\Delta t| < 2.5\,\text{ps}$; then χ_d must be modified to represent the integrated mixing probability for $|\Delta t| < 2.5$ ps. Using the world-average value for Δm_d, $0.472 \pm 0.017\ \hbar\ \text{ps}^{-1}$ [3], and taking into account the detector resolution function $\mathcal{R}(\Delta t)$, we find

$$\chi'_d = \frac{1}{2}[1 - \frac{\int_{-2.5ps}^{+2.5ps}\{e^{-|\Delta t|/\tau} cos(\Delta m_d \Delta t) \otimes \mathcal{R}(\Delta t)\} d(\Delta t)}{\int_{-2.5ps}^{+2.5ps}\{e^{-|\Delta t|/\tau} \otimes \mathcal{R}(\Delta t)\} d(\Delta t)}] = 0.079. \tag{17}$$

Solving for Eq. 16 for w, and using the calculated value for χ'_d, we obtain

$$w = \frac{\chi_{obs} - f_s \chi'_d - \sum_\beta f_\beta \chi_\beta}{f_s(1 - 2\chi'_d)}. \tag{18}$$

8.2 Results

8.2.1 Hadronic sample

The selection of hadronic B mesons was described in Section 6.1. We use all tagged events with $|\Delta t| < 2.5\,\text{ps}$, and determine the background fraction in the signal sample from a fit to the m_{ES} distribution as described in Section 7. The signal region is defined as events with $m_{\text{ES}} > 5.27\,\text{GeV}/c^2$. The fraction of mixed events in the background is determined by tag category using the sideband control sample, $m_{\text{ES}} < 5.27\,\text{GeV}/c^2$.

We use Eq. 18 to solve for the mistag rate for each tag category, obtaining the results shown in Table 8.

8.2.2 Semileptonic sample

The selection of $B \to D^* l\nu$ events was described in Section 6.3. We use tagged events with $|\Delta t| < 2.5\,\text{ps}$ and re-evaluate the backgrounds for events in this time interval, with the control samples described above. The backgrounds are evaluated for each tag category and for each D^0 decay mode. The mistag fractions are calculated individually by tag category and decay mode using Eq. 18, and the results for the different decay modes are combined, using the statistical errors

Table 8: Mistag rate w and tagging separation Q as measured by the single-bin method in the hadronic and semileptonic B event samples. The mistag rates include small corrections corresponding to the difference between the generated and reconstructed values in simulated signal events.

Tagging Category	Hadronic		Semileptonic	
	Mistag Rate w	$Q = \epsilon_{tag}(1-2w)^2$	Mistag Rate w	$Q = \epsilon_{tag}(1-2w)^2$
`Lepton`	0.120± 0.032	0.061	0.095± 0.018	0.079
`Kaon`	0.207± 0.021	0.126	0.177± 0.014	0.154
`NT1`	0.127± 0.035	0.067	0.200± 0.024	0.041
`NT2`	0.342± 0.036	0.016	0.346± 0.024	0.016
All	—	0.270	—	0.290

to weight the individual results. All systematic errors are conservatively taken to be correlated between the different decay modes. The determination of systematic errors will be discussed in the next section. The results are summarized in Table 8.

8.3 Systematic errors

The various sources of systematic error in the single-bin method that have been investigated for the hadronic and semileptonic B samples are summarized in Tables 9 and 10 and discussed in detail below.

Table 9: Sources of systematic error for the mistag measurement on the hadronic sample in the single-bin method. See text for details.

Type	Variation	`Lepton`	`Kaon`	`NT1`	`NT2`
Background	$\pm 1\sigma$	0.004	0.004	0.008	0.006
χ_d	0.174 ± 0.009	0.005	0.004	0.005	0.004
Resolution	see text	0.002	0.002	0.002	0.002
wrong tag resolution	see text	0.005	0.009	0.007	0.013
Monte Carlo correction		+0.009	+0.004	-0.026	-0.007
Monte Carlo statistics		0.012	0.008	0.017	0.015
Total		0.015	0.014	0.021	0.021

The systematic error due to background in the data samples is taken by varying both the background fractions and the fraction of mixed events associated to each background source, χ_β. These quantities are varied by one standard deviation of the values measured in the background control samples described in Section 6. For the semileptonic sample, this is the dominant source of systematic error, primarily due to the limited statistics of the background control samples.

The systematics uncertainties introduced by background from the decay $B^+ \to D^{*-} X \ell^+ \nu$ are obtained by varying the fraction described in Section 6.3 as well as the mistag fraction of the charged B meson measured on data.

The assumed Δt resolution function is a double-Gaussian where the initial parameters are taken

Table 10: Sources of systematic error for the mistag measurement from the semileptonic sample in the single-bin method. See text for details.

Type	Variation	Lepton	Kaon	NT1	NT2
Background	$\pm 1\sigma$	0.008	0.010	0.023	0.020
$B^- \to D^{*-} X \ell^+ \nu$	see text	0.009	0.009	0.009	0.008
χ_d	0.174 ± 0.009	0.012	0.009	0.009	0.004
Resolution	see text	0.002	0.002	0.002	0.002
wrong tag resolution	see text	0.005	0.009	0.009	0.013
Monte Carlo correction		0.001	-0.001	-0.003	-0.014
Monte Carlo statistics		0.010	0.006	0.013	0.012
Total		0.021	0.020	0.031	0.028

from simulation. The two widths are multiplied by two scale factors which are determined in a fit to the data along with the fraction of events in the narrow Gaussian. The double-Gaussian RMS is consistent with that of the resolution function considered in Section 7. These three parameters are varied in a conservative way within the errors of the fit to the data to determine the systematic uncertainty on the mistag fraction, which is quite small.

Finally, we consider the possibility that wrong tags have worse Δt resolution than correct tags. This effect has been studied in Monte Carlo simulation, where we observe a slightly larger RMS in the Δt distribution for events with wrong-sign tags. We assign a systematic error on the mistag rates by taking the default resolution function and changing the parameters of the resolution function for wrong tags by a corresponding amount.

9 Comparison of likelihood and single-bin methods

Combining the results obtained for the hadronic and semileptonic B samples for the likelihood fit method described in Section 7 and for the single-bin method described in Section 8, and taking into account the correlated systematic errors, we obtain the preliminary mistag rate results summarized in Table 11. The Monte Carlo corrections to the likelihood fit results summarized in Tables 6 and 7 have been applied to the likelihood fit results of Table 5.

Table 11: Combined mistag results for the hadronic and semileptonic B samples, for the likelihood and single-bin methods.

Tag Category	Mistag, w	
	Likelihood	Single-Bin
Lepton	$0.096 \pm 0.017 \pm 0.013$	$0.102 \pm 0.016 \pm 0.015$
Kaon	$0.197 \pm 0.013 \pm 0.011$	$0.187 \pm 0.012 \pm 0.015$
NT1	$0.167 \pm 0.022 \pm 0.020$	$0.176 \pm 0.020 \pm 0.024$
NT2	$0.331 \pm 0.021 \pm 0.021$	$0.345 \pm 0.020 \pm 0.023$

The single-bin fit results use a sub-sample of the events used in the likelihood fit, so the two

sets of results are correlated. The systematic errors differ, due to the different sensitivities of the two methods. Overall, the two methods agree well. The effective flavor tagging efficiency of the algorithm described in Section 5 is found to be $Q \approx 0.28$.

10 Summary

In 8.9 fb^{-1} of e^+e^- annihilation data collected near the $\Upsilon(4S)$ resonance, we have obtained a preliminary measurement of the time-dependent $B^0\overline{B}^0$ oscillation frequency using a sample of B^0 mesons reconstructed in hadronic decay channels and in the semileptonic decay mode $B^0 \to D^{*-}\ell^+\nu$.

From the hadronic B^0 sample we measure the $B^0\overline{B}^0$ oscillation frequency:

$$\Delta m_d = 0.516 \pm 0.031 \text{ (stat.)} \pm 0.018 \text{ (syst.)} \ \hbar \text{ ps}^{-1}$$

From the $D^{*-}\ell^+\nu$ sample we measure the $B^0\overline{B}^0$ oscillation frequency:

$$\Delta m_d = 0.508 \pm 0.020 \text{ (stat.)} \pm 0.022 \text{ (syst.)} \ \hbar \text{ ps}^{-1}$$

Combining the Δm_d results from the hadronic and semileptonic B samples, we obtain the preliminary result :

$$\Delta m_d = 0.512 \pm 0.017 \text{ (stat.)} \pm 0.022 \text{ (syst.)} \ \hbar \text{ ps}^{-1}.$$

In combining the two results, we have taken all systematic error contribution to be fully correlated with the exception of the contribution due to Monte Carlo simulation statistics.

11 Acknowledgments

We are grateful for the contributions of our PEP-II colleagues in achieving the excellent luminosity and machine conditions that have made this work possible. We acknowledge support from the Natural Sciences and Engineering Research Council (Canada), Institute of High Energy Physics (China), Commissariat à l'Energie Atomique and Institut National de Physique Nucléaire et de Physique des Particules (France), Bundesministerium für Bildung und Forschung (Germany), Istituto Nazionale di Fisica Nucleare (Italy), The Research Council of Norway, Ministry of Science and Technology of the Russian Federation, Particle Physics and Astronomy Research Council (United Kingdom), the Department of Energy (US), and the National Science Foundation (US). In addition, individual support has been received from the Swiss National Foundation, the A. P. Sloan Foundation, the Research Corporation, and the Alexander von Humboldt Foundation. The visiting groups wish to thank SLAC for the support and kind hospitality extended to them.

References

[1] UA1 Collaboration, C. Albajar *et al.*, Phys. Lett. **B186** (1987) 247.

[2] ARGUS Collaboration, H. Albrecht *et al.*, Phys. Lett. **B192** (1987) 245.

[3] D.E. Groom, *et al.*, Eur. Phys. Jour. C **15**(2000) 1.

[4] M. Kobayashi and T. Maskawa, Prog. Theor. Phys. **49** (1973) 652.

[5] *BABAR* Collaboration, B. Aubert *et al.*, "A study of time-dependent *CP*-asymmetries in $B^0 \to J/\Psi K^0_S$ and $B^0 \to \Psi(2S)K^0_S$ decays", *BABAR*-CONF-00/01, submitted to the XXXth International Conference on High Energy Physics, Osaka, Japan.

[6] *BABAR* Collaboration, B. Aubert *et al.*, "The first year of the *BABAR* experiment at PEP-II", *BABAR*-CONF-0017, submitted to the XXXth International Conference on High Energy Physics, Osaka, Japan

[7] G. C. Fox and S. Wolfram, Phys. Rev. Lett. **41**(1978) 1581.

[8] *BABAR* Collaboration, B. Aubert *et al.*, "Exclusive B decays to charmonium final states", *BABAR*-CONF-0005, submitted to the XXXth International Conference on High Energy Physics, Osaka, Japan

[9] ARGUS Collaboration, H. Albrecht *et al.*, Phys. Lett. **B185** (1987) 218.

[10] ALEPH Collaboration, D. Buskulic, *et al.*, Z. Phys. **C73** (1997) 601; DELPHI Collaboration, P.Abreu, *et al.*, Phys. Lett. **B475** (1999) 407.